



19941228 002

ANALYSIS OF INSTABILITY GROWTH AND  
COLLISIONLESS RELAXATION IN THERMIONIC  
CONVERTERS USING 1-D PIC SIMULATIONS

THESIS

Bret B. Kreh, Lieutenant, USAF

AFIT/GAP/ENP/94D-06

**DISTRIBUTION STATEMENT A**

Approved for public release  
Distribution Unlimited



DEPARTMENT OF THE AIR FORCE  
AIR UNIVERSITY

**AIR FORCE INSTITUTE OF TECHNOLOGY**

Wright-Patterson Air Force Base, Ohio

AFIT/GAP/ENP/94D-06

ANALYSIS OF INSTABILITY GROWTH AND  
COLLISIONLESS RELAXATION IN THERMIONIC  
CONVERTERS USING 1-D PIC SIMULATIONS

THESIS

Bret B. Kreh, Lieutenant, USAF

AFIT/GAP/ENP/94D-06

DTIC QUALITY INSPECTED 2

Approved for public release; distribution unlimited

The views expressed in this thesis are those of the author and do not reflect the official policy or position of the Department of Defense or the U.S. Government

Accession For	
NTIS GRA&I	<input checked="" type="checkbox"/>
DTIC TAB	<input type="checkbox"/>
Unannounced	<input type="checkbox"/>
Justification	
By _____	
Distribution/ _____	
Availability Codes	
Dist	Avail and/or Special
A-1	

AFIT/GAP/ENP/94D-06

ANALYSIS OF INSTABILITY GROWTH AND COLLISIONLESS RELAXATION  
IN THERMIONIC CONVERTERS USING 1-D PIC SIMULATIONS

THESIS

Presented to the Faculty of the School of Engineering  
of the Air Force Institute of Technology  
Air University  
In Partial Fulfillment of the  
Requirements for the Degree of  
Master of Science

Bret B. Kreh, B.S.  
Lieutenant, USAF

December 1994

Approved for public release; distribution unlimited

## *Preface*

Thermionic converters are a reliable and promising source of power for space-based systems. If these devices are to be used in the future, we must understand how they work and why they behave the way they do. Without a detailed understanding of the processes in the devices, there can be no true optimization.

In an effort to expand this knowledge, I endeavored to explore the rate of collisionless relaxation in determining the operating characteristics of these devices. I was able to show that these phenomena, manifested in the form of velocity space instabilities, grow fast enough in a simplified system to be an important factor and competitive with collisional effects. If these instabilities are to be better quantified, parameterized, and geometric limitations incorporated, more work must be done.

I would like to acknowledge the help and guidance provided to me by my advisor, Dr. Bailey. His willingness to help me understand the problem, although it sometimes meant staying late, is a credit to him. I am also grateful to Capt. Nichols for his patience in answering my questions and providing help with the simulation code, even as he was working on his dissertation.

Finally, I would like to thank all my friends in the Physics department for putting up with my frustrated ramblings. I am grateful to all who lent a sympathetic ear to my complaints. I wish the best of luck to them all in their future endeavors.

## *Table of Contents*

	<i>page</i>
Preface _____	ii
Table of Contents _____	iii
List of Figures _____	iv
List of Table _____	vi
List of Symbols _____	vii
Abstract _____	ix
I. Introduction _____	1
II. Background _____	3
III. Theory _____	15
IV. Comparison with Simulations _____	29
V. Discussion and Conclusions _____	43
Appendix A: Definition of Quantities in the ES1 Input Deck _____	48
Appendix B: Definition of Quantities in the PDP1 Input Deck _____	51
References _____	55
Vita _____	57

## *List of Figures*

Figure		Page
1.	Thermionic Converter Configuration _____	3
2.	Potential for a Thermionic Converter with an External Load _____	4
3.	J-V curves showing the modes of operation for a plasma diode (load voltage increasing to the left) (11:1194) _____	6
4.	Potential for the Diffusion Mode (dash-dot), Ignition transition (dotted), and Ignited Mode(solid) _____	8
5.	A) Emission Electron Distribution, B) Emitted Beam After Acceleration Through Cathode Sheath, and C) Bulk Plasma Electron Distribution _____	11
6.	Periodic Distribution of the Potential Energy in the Wave Frame _____	13
7.	Dispersion Diagram for Cold Plasma Oscillations _____	19
8.	Cold Plasma Oscillations for Drifting Plasmas with Velocities $v$ (solid), $2v$ (dashed), and $-v$ (dotted) _____	19
9.	Dispersion Relation for Symmetric Two-Stream Interaction Compared to Drifting Cold Plasma Oscillations _____	20
10.	Imaginary Portion of Solutions to the Symmetric Two-Stream Dispersion Relation _____	21
11.	Imaginary portion of $\tilde{\omega}$ vs. normalized velocity, $\tilde{v}$ , for modes 1-3, from right to left _____	22
12.	Modes 4-13(right to left) for Two-Stream Instability, $\gamma=1$ _____	23
13.	Dispersion Relation Solutions for Beam-Plasma Interaction, $\gamma=1$ , Compared to Independent Cold Plasma Oscillations _____	25
14.	Modes 13-22(right to left) for Beam-Plasma, $\gamma=1$ _____	25

15.	Dispersion surface , $\frac{\omega}{\omega_{p\alpha}}$ ,for beam-plasma interaction. $\tilde{\nu}$ ranges from 0 to 10, and $\gamma$ ranges from 0 to 20	27
16.	Dispersion curve for beam-plasma interaction for $\gamma=1$ (dashed), and for $\gamma=7.07$ (solid)	27
17.	Fit to data for mode 1 growth in ES1 with $\tilde{\nu} = 0.8660$	33
18.	Snapshot of ES1 Sub-Threshold Behavior.	34
19.	Snapshot of ES1 Instability onset	35
20.	Mode 3 data for two-stream interaction with $\tilde{\nu}=1, \gamma=1$ and a) only mode 1 stimulated, and b) modes 1-3 stimulated	36
21.	Fit to data (dots) compared to analytical curves for two-stream interaction, $\gamma=1$ , modes 1-3	37
22.	Snapshot of PDP1 Run for Electron-Electron Two-Stream Interaction $\gamma=1, v=7.9 \times 10^5$ m/sec at $t=3.98 \times 10^{-10}$ seconds	41
23.	Snapshot of PDP1 Run for Electron-Electron Two-Stream Interaction $\gamma=1, v=7.9 \times 10^5$ m/sec at $t=9.96 \times 10^{-10}$ seconds	42

*List of Tables*

Table	Page
1. Growth Rates for Modes 4-13 for the Two-Stream Instability with $\gamma=1$ _____	23
2. Growth Rate for Modes 13-22 for Beam-Plasma Interaction with $\gamma=1$ _____	26
3. Growth Rate for Modes 76-85 for Beam-Plasma Interaction with $\gamma=7.07$ _____	28
4. Fit, Predicted Values and Relative Error for Beam-Plasma Interaction, $\gamma=1$ _____	38
5. Growth Rates for Electron-Electron Beam-Plasma, $\gamma=1$ , Modes 13-22 _____	39
6. Growth Rates for Electron-Electron Beam-Plasma, $\gamma=7.07$ , modes 76-85 _____	40

## *List of Symbols*

$h$	Planck's constant
$k_B$	Boltzmann's constant
$m_e$	electron mass
$q_e$	electron charge
$\phi$	cathode work function
$\epsilon_0$	permittivity of free space
$n_\alpha$	number density for species $\alpha$
$n_\beta$	number density for species $\beta$
$v_\alpha$	velocity for species $\alpha$
$v_\beta$	velocity for species $\beta$
$q_\alpha$	charge of a particle in species $\alpha$
$q_\beta$	charge of a particle in species $\beta$
$\omega_{p\alpha}$	plasma frequency for species $\alpha$
$\omega_{p\beta}$	plasma frequency for species $\beta$
$\omega_p$	plasma frequency $\left( \sqrt{\frac{n}{m\epsilon_0}} q_e \right)$
$\gamma$	$\frac{\omega_{p\beta}}{\omega_{p\alpha}}$
$\tilde{\omega}$	$\frac{\omega}{\omega_{p\alpha}}$
$\tilde{v}$	normalized velocity $\left( \frac{kv}{\omega_{p\alpha}} \right)$
$k$	wave number
$k_N$	wave number of mode N
$\omega$	angular frequency

$n$	number density
$L$	length of system (electrode spacing)
$E$	electric field
$j$	current density

*Abstract*

This work investigates the role that the beam-plasma instability may play in a thermionic converter. The traditional assumption of collisionally dominated relaxation is questioned, and the beam-plasma instability is proposed as a possible dominant relaxation mechanism. Theory is developed to describe the beam-plasma instability in the cold-plasma approximation, and the theory is tested with two common Particle-in-Cell (PIC) simulation codes.

The theory is first confirmed using an unbounded plasma PIC simulation employing periodic boundary conditions, ES1. The theoretically predicted growth rates are on the order of the plasma frequencies, and ES1 simulations verify these predictions within the order of 1%. For typical conditions encountered in thermionic converters, the resulting growth period is on the order of  $7 \times 10^{-11}$  seconds.

The bounded plasma simulation PDP1 was used to evaluate the influence of finite geometry and the electrode boundaries. For this bounded plasma, a two-stream interaction was supported and resulted in nearly complete thermalization in approximately  $5 \times 10^{-10}$  seconds. Since the electron-electron collision rate of  $10^9$  Hz and the electron atom collision rate of  $10^7$  Hz are significantly slower than the rate of development of these instabilities, the instabilities appear to be an important relaxation mechanism.

# ANALYSIS OF INSTABILITY GROWTH AND COLLISIONLESS RELAXATION IN THERMIONIC CONVERTERS USING 1-D PIC SIMULATIONS

## *I. Introduction*

As we continue to push into space, the need for compact and lightweight power sources becomes ever more pressing. Devices that convert heat to electrical energy by means of thermionic emission have been proposed to fill this need (9:94). Though by no means the only reason to explore the physics of thermionic devices, such an application raises an interest in the behavior and optimization of this power conversion method.

With the increased interest in thermionic devices comes the need to understand the mechanisms of their operation. Numerical models have been developed, but fall short of predicting some important details of device behavior. Improving the predictive capabilities of the models will enhance the understanding of the devices, and allow for greatly improved designs.

With this goal in mind, this work is a study of the plasma dynamics in thermionic converters. The focus is on interactions which may play an important role in the behavior of the device at the optimum power point. Specifically, the beam-plasma instability is investigated as a possible major contributor to the thermalization of the injection stream in a converter, and hence a determining factor in device characterization. The plasma fluid equations are used to discuss, analyze, and establish instability growth rates for conditions representative of the saturated and obstructed regimes of a thermionic converter. The analytical growth rates are compared to those observed in computer simulation experiments using ES1, electrostatic 1-dimensional code, a one-dimensional particle-in-

cell (PIC) code with periodic boundary conditions (14:1-20). PDP1, plasma device planar 1-dimensional bounded electrostatic code, is used to investigate the effects of bounding the plasma (15:1-31). These results are summarized and interpreted in terms of existing conditions in the ignited mode of a thermionic converter.

Chapter II will establish the background for this research project, providing a brief description of thermionic converters. The behavior of a plasma in these devices is explored. Chapter III contains a derivation of the equations describing the instabilities considered in this work. In Chapter IV, the PIC approach is described, along with an overview of the ES1 and PDP1 codes. PIC simulations are then used to verify the analytically established instability growth rates of Chapter III. In Chapter V, the implications of these equations are explored for a real device. The growth rates for the instabilities are compared to the collision rates, and the relative importance is discussed. Finally, some recommendations for further study are proposed.

## II. Background

Thermionic converters are power conversion devices. They convert thermal energy to electrical energy by means of thermionic emission. One of the advantages of thermionic converters is that they can operate at relatively high temperatures on both the cathode and the anode (1:4). In the space environment, radiative cooling is the only method of heat rejection available, and the radiated power per unit area is proportional to  $T^4$ . Consequently, as the temperature of the radiator increases, the area needed to radiate the same amount of power is drastically reduced. As the area is reduced, the weight of the system can be reduced. Given the high temperature operating characteristics of thermionic converters, thermionic based power systems can be made smaller and lighter than other power systems.

Thermionic converters consist of a cathode (or emitter), with a work function  $\phi_c$ , anode (or collector), with a work function  $\phi_A$ , and an external circuit as seen in Figure 1. The cathode is heated to a high temperature, typically 1700 K, while the anode, a short

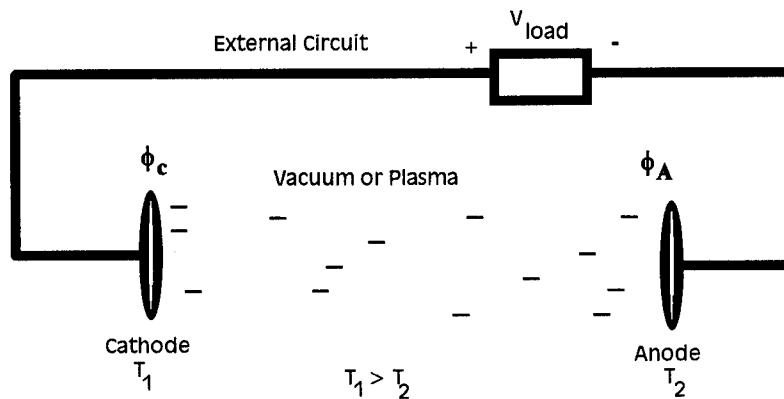


Figure 1: Thermionic Converter Configuration

distance away, is kept at a lower temperature, in the range of 1000 K. The electrons emitted from the cathode have the potential energy equivalent to the work function of the cathode, typically made of tungsten with a work function of around 5 eV (1:34). Since

the anode typically has a lower work function than the cathode, there is a net accelerating potential for the electrons as shown in Figure 2 (10:7). In order to extract the power from

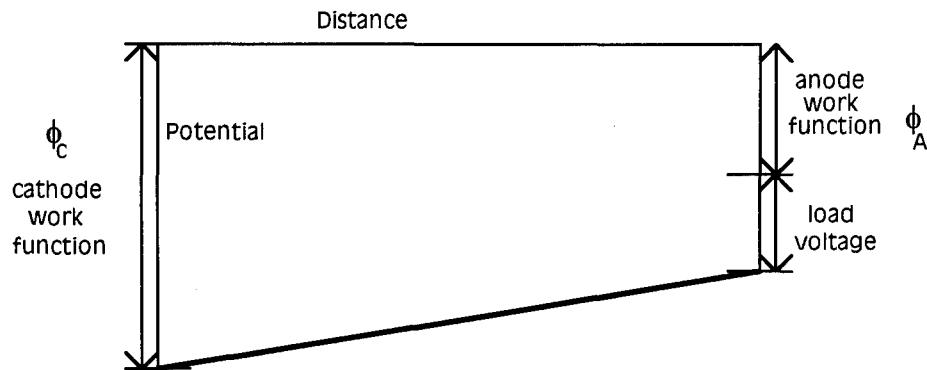


Figure 2: Potential for a Thermionic Converter with an External Load.

the converter, a load is placed in the external circuit. The voltage developed across this load will be referred to as the load voltage.

To understand the behavior of thermionic devices, it is easiest to start with the concept of the ideal diode. In the ideal diode, so long as the sum of the load voltage and the anode work function does not exceed that of the cathode work function, there is nothing to prevent all of the electrons emitted from crossing the gap. The current across the device is therefore equal to the cathode emission current given by Richardson's equation (8:148):

$$j = \frac{4 \cdot \pi}{h^3} m_e k_B^2 q_e T^2 \cdot e^{q_e \phi_c / kT} \quad (1)$$

where  $k_B$  is Boltzmann's constant,  $h$  is Planck's constant,  $\phi_c$  is the cathode work function,  $T$  is the cathode temperature, and  $m_e$  and  $q_e$  are the electron charge and mass respectively. Because this current depends only on the temperature and work function of the cathode, it remains constant for all voltages satisfying the restriction:  $V_{load} < \phi_c - \phi_A$ .

When the sum of the anode work function and the load voltage does exceed the cathode work function, the electrons must lose kinetic energy to cross the gap. The number crossing the gap and therefore contributing to the current depends on the form of

the electron distribution function upon emission. In a thermionic device, the emitted electrons can be approximately characterized by a half-Maxwellian distribution with a temperature equal to that of the cathode (4:6). This means that as the load voltage is increased beyond the difference between the cathode and anode work functions, the number of electrons with sufficient kinetic energy to cross the gap decreases exponentially, and thus the current across the device does as well.

Reality is not as simple as the ideal diode. When the space between the anode and the cathode is in vacuum, the emitted electrons, in the process of crossing the interelectrode gap, form a space charge which impedes the current flow. To minimize this effect, the electrode separation can be made very small or, alternatively, the space can be filled with a positive ion source, neutralizing the space charge. If the space charge effect is to be minimized by changing the interelectrode space, consistent with the Langmuir-Childs equation, the spacing must be on the order of a few microns. Since manufacturing and maintaining at tolerance a spacing this narrow between two large, heated surfaces is very difficult, the most commonly used converters use a plasma to neutralize the space charge (1:5-6).

Ionization of a gas, introduced into the interelectrode space provides a positive ion source to help counter the negative space charge from the emitted electrons. Cesium is most commonly used because of its low ionization potential (1:6). In a plasma diode, there are two mechanisms for ionization: surface and volume ionization. The work function of the cathode is higher than the ionization potential of cesium, and thus when an atom contacts the hot cathode, it is ionized. This is known as surface ionization. Volume ionization proceeds via electron impact in the bulk region and dominates at the high plasma densities and temperatures. Because cesium has a low ionization potential, the threshold for dominance of volumetric ionization is lower in cesium than it is for other gases. Therefore, volume ionization onsets at lower energies for cesium than for other gases in a thermionic device.

Neutralizing the space charge is not the only benefit cesium provides in a thermionic device. Cesium also bonds to the surface of the cathode and lowers the cathode's effective work function, increasing the emission current (1:11,30-33). Thus the addition of cesium into the device helps to increase the current both by neutralizing the space charge and by increasing the emission current.

With the addition of the plasma, however, the device becomes more difficult to characterize. For a cesium diode, there are two modes of operation: unignited or diffusion mode, and the ignited mode. The ignited mode can be divided into two regimes, saturated and obstructed, with the boundary identified as the transition point (Figure 3). First, a quick overview of these regimes will be given, with a more detailed description to be given later.

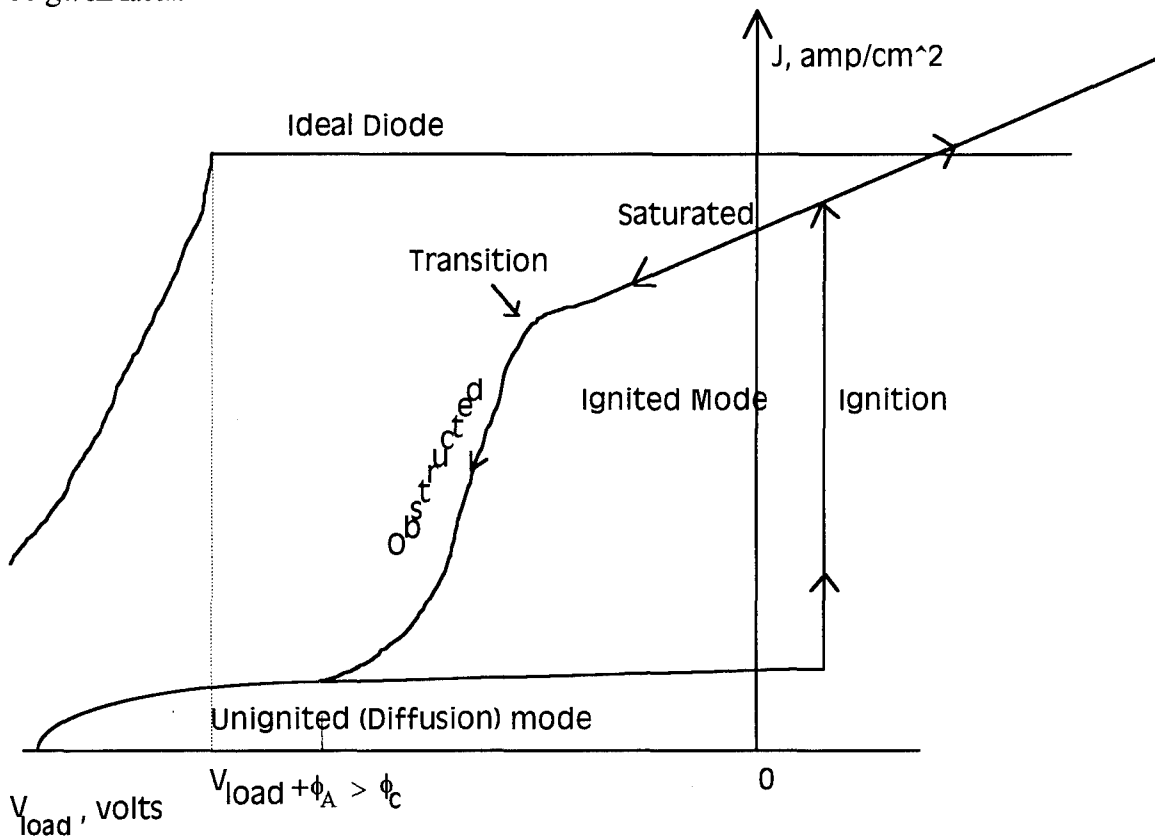


Figure 3: J-V curves showing the modes of operation for a plasma diode(load voltage increasing to the left) (11:1194)

If the device is operated with a fairly high load voltage, it will be in the unignited mode, as depicted in the lower curve of Figure 3. The unignited, or diffusion, mode has a very low current, typically on the order of  $10 \text{ mA/cm}^2$ , which remains relatively constant with voltage. However, at a high enough load voltage, the electrons emitted from the cathode are prevented from crossing the device, and the current is zero. Throughout the remaining range of operating voltages the current is virtually unaffected.

When the load voltage is reduced below the ignition point, which may require an applied voltage, there is an abrupt jump in the amount of current flowing, as identified by the vertical arrow in Figure 3. The new, high current mode is the ignited mode. The high current regime existing at relatively low load voltages in the ignited mode is the saturated regime. In the saturated regime, nearly all of the electrons emitted at the cathode make it across the device. Losses in the plasma can reduce the current below that predicted for the ideal diode. However, the current in the saturated regime can exceed that predicted for the ideal diode when a large enough electric field forms just outside the cathode. This accelerating electric field effectively lowers the work function of the cathode and enhances emission in what is known as the Schottky effect. When this increase is larger than the losses in the plasma, the current will exceed that predicted for the ideal diode.

If we move down the J-V characteristic curve toward the higher load voltages, meaning a reduction in the total potential across the device, the curve passes through the "knee" or transition point, and the current then begins to drop much more rapidly with increasing load voltage. This behavior is reminiscent of the exponential decrease in the ideal diode and is known as the obstructed regime. The accepted explanation for the loss in current is that a potential barrier forms just in front of the cathode (10:16-19), reflecting the majority of emitted electrons back to the cathode.

Now that the general description of the regimes on the J-V curve has been given, the behavior in these regimes can be explored in a little more depth. The unignited (diffusion) mode is characterized by a relatively low and nearly constant current. In this

mode, the electrons have insufficient energy to ionize the atoms and thus surface ionization is the sole source of positive ions. These ions are then drawn into the device by the combined effects of the space charge and diffusion. In the diffusion mode, the interelectrode potential remains virtually level except for a narrow sheath near the anode and a small sheath near the cathode, with a potential drop on the order of the cathode temperature, as shown by the dash-dot line in Figure 4. The associated weak electric field and the low surface ionization rate result in the low currents characteristic of this mode.

Even with a reduction of the load voltage, and thus an increase in the potential across the device, large potential gradients do not arise in the bulk region of the device. A large potential difference in the bulk region of the plasma would prevent the ions from making it across the device. A negative space charge would then develop between the furthest point the ions reached and the collector, but this would draw the ions further across the device. Eventually, the potential will be too steep for a significant space charge to develop, and the majority of the potential drop will be in the sheath near the anode. So, in the diffusion mode, the potential remains relatively flat except for a narrow region just outside the anode known as the anode sheath.

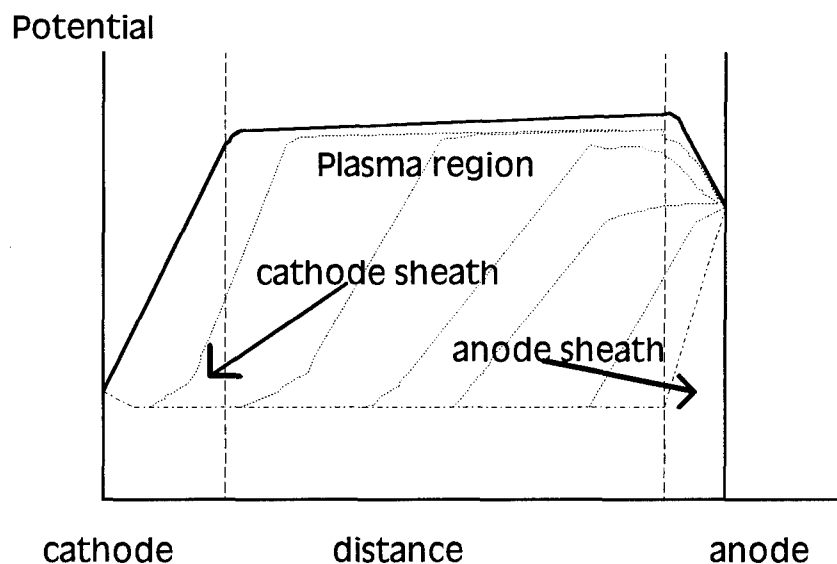


Figure 4: Potential for the Diffusion Mode (dash-dot), Ignition transition (dotted), and Ignited Mode(solid).

With a sufficient potential across the device, the anode sheath is high enough and steep enough to give the electrons entering it the energy required to ionize the gas. When the voltage reaches the point of ignition on Figure 3, the local rate of ion production in the sheath exceeds the rate at which the ions are convectively removed. As the positive ions accumulate near the anode, they raise the potential in this region and push the accelerating potential further into the device toward the cathode. This "wave" of volumetric ionization progresses across the gap, as shown by the dotted lines, and continues until the convective loss of the ions to the electrodes is just balanced by the creation of new ions. The potential configuration at the end of this transition to the ignited mode is depicted in Figure 4 with a solid line.

The potential profile illustrated in Figure 4 with the solid line is characteristic of the saturated regime. In this regime, the device can be divided into three basic regions. The region near the cathode where the potential rises steeply is referred to as the cathode sheath. This region is a few Debye lengths wide for a typical converter in the saturated mode, approximately  $3 \times 10^{-5}$  m (10:68). The relatively flat portion in the potential occupying the majority of the device is known as the plasma or bulk region. Here, the ions have created a quasi-neutral, weak field region. Continuity of current implies a small net drift in this region. Because of the larger density in the plasma region, the drift velocity of the plasma is negligible compared to the velocity of the emitted beam of electrons accelerated through the cathode sheath. A second sheath region in the vicinity of the anode is formed to preserve the neutrality of the plasma and maintain continuity of current flow. This anode sheath is also on the order of a Debye length in width with a fall voltage of the order of the plasma electron temperature.

The character of the potential is altered with higher load voltages. With sufficient load voltage, the device enters into the obstructed mode. The true nature of this mode is not well understood, and this may lead to many of the predictive failures of the numerical models (10:15-19). The currently accepted explanation for the drop in current in the

obstructed mode is that a potential barrier forms just outside the cathode (1:298,333-335). This potential barrier reduces the current by blocking the slower electrons from entering into the plasma. Because the most energetic electrons can cross the barrier and the net energy gained in the cathode sheath remains approximately the same, the rate of volumetric ionization can still be sustained for a range of load voltages in the obstructed regime. However, as the load voltage is further increased, the barrier in front of the cathode also increases. When this barrier becomes large enough, so few electrons traverse the sheath and enter the plasma that it is no longer possible to sustain the volumetric ionization, and the plasma collapses back into the diffusion mode.

The power produced by a thermionic device is dependent on supplying both large current and a large load voltage. Since larger load voltages lead to lower currents, it is important to find an optimal operating regime. Because the current is so low in the diffusion mode, operation in this mode is not very efficient. In the ignited mode, the saturated regime has the largest current, but this current is sustained only at low load voltages. In contrast, the obstructed regime voltages are higher, but current diminishes rapidly with increasing voltage. As a result, the optimal power output is found between the obstructed and saturated regimes, at the transition point as labeled in Figure 3 (10:15).

To more accurately characterize device operation at the optimal power point, the sheath structure and plasma behavior must be understood. In pursuit of this goal, there are two general theoretical approaches to formulating the equations describing the behavior of a plasma in a thermionic converter. The microscopic, or kinetic, method requires the solution of the Boltzmann equation directly, and can be quite complex. The macroscopic, or fluid, description offers a more simplified view of the plasma. Both of these methods have their strengths and weaknesses.

The microscopic approach emphasizes the discrete nature of the plasma. The plasma is described by the position and velocity of individual particles. This method can

accurately capture most of the behaviors of the plasma in a thermionic converter, but can also be cumbersome and computationally intensive.

To simplify this picture, the plasma will often be described in terms of the macroscopic quantities such as charge and particle densities, mean velocities and energies, rather than with the individual particle locations and velocities. Moments of the kinetic equation produce a set of equations, the hydrodynamic or fluid equations, in these macroscopic quantities. This simplification facilitate analysis while sacrificing the generality of approach. The accuracy of the results is much more sensitive to the assumptions made in deriving them, specifically local equilibrium with the electric field and the assumed form of the distribution function.

In Figure 5, the interelectrode potential in the ignited mode of a thermionic converter is re-introduced, with the purpose of identifying the characteristic form of the electron velocity distribution at the cathode surface (A), after acceleration in the cathode sheath (B), and in the bulk plasma region (C). Electrons are emitted from the cathode with a thermal distribution equivalent to the cathode temperature, typically 1700 K. They are then accelerated through the cathode sheath of approximately 1 V. Approximating the

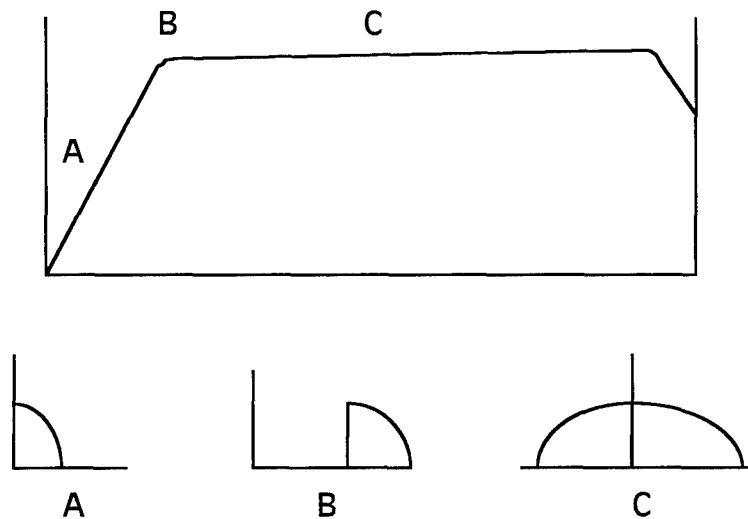


Figure 5: A) Emission Electron Distribution, B) Emitted Beam After Acceleration Through Cathode Sheath, and C) Bulk Plasma Electron Distribution.

emission electron velocity distribution as a half-Maxwellian, (A), the electrons leave the cathode with an average drift velocity of  $2.0 \times 10^5$  m/sec. The acceleration through the 1 V cathode sheath adds a drift velocity of  $5.9 \times 10^5$  m/sec. Combining the average drift from the half-Maxwellian thermal distribution and the added drift velocity from the 1 V acceleration, the emission electrons have an average drift velocity of about  $7.9 \times 10^5$  m/sec as they enter the bulk region of the plasma. For a typical converter, the plasma density is around  $5 \times 10^{19} \text{ m}^{-3}$  and the plasma electron temperature is 2400 K. The electron-electron and electron-ion collision frequencies for these plasma conditions are on the order of  $10^9$  Hz and  $10^7$  Hz, respectively, with electron-neutral collisions even less frequent (10:20). These conditions translate to a mean free path on the order of  $7.9 \times 10^{-4}$  m for electron-electron collisions, and  $7.9 \times 10^{-2}$  m for electron-ion collisions. However, the typical converter has an interelectrode spacing on the order of  $5 \times 10^{-4}$  m. The mean free path for electron-electron collisions is of the same order as the device dimension, and the electron-ion mean free path is two orders of magnitude higher. Considering these characteristic lengths, it is difficult to attribute the thermalization of the electron beam, (B) to (C) in Figure 5, to either electron-neutral or Coulomb collisions. However, collisionless interactions may account for the relaxation of the emitted beam to the thermal distribution associated with the plasma region. This project is the study of these collisionless relaxation mechanisms, which may dominate or augment the collisional relaxation.

The collisionless interaction most likely to play a significant role in a thermionic converter is the beam-plasma instability. The beam-plasma instability arises from an exchange of energy between an energetic beam of electrons, like the emission electrons exiting the cathode sheath, and a quiescent plasma, similar to that found in the bulk plasma region of the converter. As a brief introduction to the physics of the beam-plasma interaction, Seshadri used a semi-quantitative argument to describe this exchange of energy, and this argument will be closely followed here (13:135-140). Consider a plasma

where the ions are so heavy as to be immobile. In this plasma, the electric field is slightly perturbed by a longitudinal wave of the form  $E(x,t)=E_0\sin(kx-\omega t)$ .

If the coordinate system is redefined to be traveling at the phase velocity of the wave. The wave will therefore appear stationary and can be described by  $E(x)=E_0\sin kx$ . Without loss of generality,  $E_0$  is assumed to be positive. Now, since the wave is stationary in this reference frame, a scalar potential can be defined, and is found to be:

$$\phi(x) = \frac{-E_0}{k} [1 - \cos kx] \quad (2)$$

and the potential energy is:

$$\Phi(x) = \frac{q_e E}{k} [1 - \cos kx] \quad (3)$$

where the integration constant is set such that the minimum potential is zero. The potential given by Equation (3) is a periodic set of potential wells with a height of  $2q_e E/k$ , as illustrated by Figure 6. Both the plasma and the beam are assumed to initially have a uniform velocity distribution, independent of position.

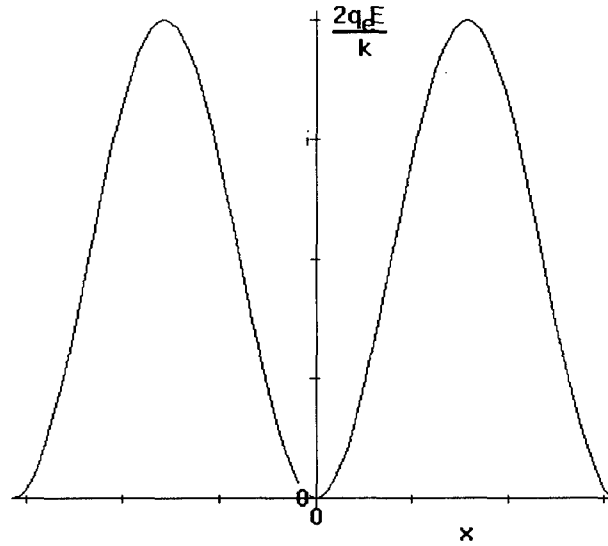


Figure 6: Periodic Distribution of the Potential Energy in the Wave Frame.

Those electrons traveling in the stationary frame at the phase velocity of the wave are stationary in the wave frame and see a constant potential, thereby remaining unaffected by the wave. However, if the electron is traveling faster than the phase velocity, it will

move across the potential. Suppose an electron is traveling at slightly faster than the wave, and starts at the bottom of one of the potential wells. This electron has a velocity in the wave-frame of  $v-v_{ph}$ , where  $v$  is the velocity of the electron and  $v_{ph}$  is the phase velocity of the wave, both in the stationary frame. Therefore the electron has an energy of  $E=m_e(v-v_{ph})^2$ . If this energy is greater than the height of the potential,  $2q_e E/k$ , than it will continue across the wave with the same average velocity, but with a sinusoidal variation in its velocity. However, if the electron's energy is less than the height of the potential, it will be trapped inside the potential well. This trapped electron will oscillate inside the well, with a net velocity of zero in the wave frame. Effectively, the electron has given its energy to the wave.

Now, consider an electron traveling slower than the wave, also at the bottom of a potential well. If the energy,  $E=m_e(v-v_{ph})^2$ , is larger than the potential height, this electron will continue to travel across the wave with no net loss in velocity, but a with a sinusoidal perturbation. However, if the energy of the electron is smaller than the potential height, it will again be trapped. This electron will now travel with an average velocity equal to the phase velocity of the wave, and has, therefore, gained energy from the wave.

From this semi-quantitative argument, it can be seen that a longitudinal oscillation in the electric field in a plasma will perturb the velocities of the electrons. Those electrons with velocities sufficiently different from the phase velocity of the wave will be perturbed, but continue to travel with their original average velocity. Electrons with velocities near the phase velocity of the wave, however, are more strongly affected, and can become trapped. This trapping leads to an exchange in energy between the wave and the electron. The alterations in the velocity also lead to "bunching," or local changes in the number density of the electrons. This bunching takes on the same sinusoidal character as the velocity perturbation causing it. A more detailed, mathematical development of the interaction follows in Chapter III.

### *III. Theory*

In the previous chapter, the basic physics of a thermionic converter was explored. The interelectrode potential and electron velocity distributions for the ignited mode were introduced. The efficiency of a collisionally based thermalization process was called into question and the collisionless beam-plasma interaction was suggested as a possible major contributor to the thermalization of the emission beam. In this chapter, the equations describing the basis of this interaction will be derived. The validation, via computer simulation, of the theory developed here will be performed in Chapter IV.

We begin by deriving the fluid equations. These equations will be used to describe the general class of collisionless interactions known as the two-stream interaction. The implications of the two-stream interaction will be explored, with the symmetric two-stream interaction used as an example. The general equations for the two-stream will be modified to give the equations for the beam-plasma interaction. The beam-plasma interaction will be considered first for beam and plasma of equal densities, and then the effect of a higher plasma density, weak beam, will be considered.

As was noted in Chapter II, there are two approaches to deriving the equations of motion for a plasma. The first method, the kinetic approach, concentrates on the microscopic quantities of the plasma, and involves a direct solution of the Boltzmann transport equation. Here, to simplify the calculation, we use the second method, the fluid equations. The plasma is treated as a number of inter-penetrating fluids. For instance, the plasma ions are one fluid, the plasma electrons are another, and the beam electrons are a third. The equations of motion for these fluids, known as the fluid equations, are expressed in terms of the macroscopic quantities of the fluids such as density, particle flux, and current density. These quantities are derived from the single particle distribution function (5:82).

For a more complete development of the fluid approach, see chapters three through five in Krall and Trivelpiece (5:78-286). A brief summary will be given here. The fluid equations are derived from the velocity moments of the Boltzmann equation. By integrating this equation over all velocity space, one obtains the continuity equation:

$$\frac{\partial}{\partial t}(\mathbf{n}_\alpha) + \nabla \cdot (\mathbf{n}_\alpha \mathbf{v}_\alpha) = 0 \quad (4)$$

where  $\mathbf{n}_\alpha$  is the number density of species  $\alpha$  and  $\mathbf{v}_\alpha$  is the velocity of species  $\alpha$ .

Integrating the product of the kinetic equation and the momentum of a particle of species  $\alpha$ , results in the momentum transfer equation:

$$\mathbf{n}_\alpha m_\alpha \left( \frac{\partial}{\partial t} + \mathbf{v}_\alpha \cdot \nabla \right) \mathbf{v}_\alpha = \mathbf{n}_\alpha q_\alpha \left( E + \frac{\mathbf{v}_\alpha \times B}{c} \right) - \nabla \cdot \Pi - \nabla p_\alpha - \int \bar{\mathbf{n}}_\alpha m_\alpha \mathbf{v} \frac{\partial f_\alpha}{\partial t} \Big|_c d\mathbf{v} \quad (5)$$

Where  $E$  is the electric field,  $m_\alpha$  and  $q_\alpha$  are the mass and charge of a particle of species  $\alpha$ ,  $\Pi$  are the off-diagonal elements of the pressure tensor,  $p_\alpha$  are the diagonal elements of the pressure tensor of species  $\alpha$ , and  $\frac{\partial f_\alpha}{\partial t} \Big|_c$  is the effective collision rate. Invoking the “cold

plasma” approximation and neglecting the contribution of collisions and magnetic field, the momentum transfer equation simplifies to:

$$\mathbf{n}_\alpha m_\alpha \left( \frac{\partial}{\partial t} + \mathbf{v}_\alpha \cdot \nabla \right) \mathbf{v}_\alpha = \mathbf{n}_\alpha q_\alpha E \quad (6)$$

The continuity and momentum transfer equations will be used with a first order perturbation analysis to derive the equations for cold plasma oscillation, and then the class of collisionless interactions known as a two-stream interaction. The beam-plasma interaction is a sub-class of this type of interaction. The two-stream interaction uses two drifting beams of particles with different velocities and possibly different masses, density, and charge. The general equations describing the two-stream interaction will be derived first and later refined to specifically address the beam-plasma interaction.

First, consider two species,  $\alpha$  and  $\beta$ , which may have different number densities, charge, velocities and mass. The electric field is perturbed slightly such that there are small oscillations about a steady state solution,  $E_{\text{tot}} = E_0 + E e^{i(kx - \omega t)}$ . As demonstrated in

chapter II, this perturbation in the electric field causes a similar perturbation in the number density and velocities for the species. The total number density and the velocities for species  $\alpha$  can then be represented by:

$$n_{\alpha \text{tot}} = n_{\alpha} + n_{\alpha 1} e^{ikx - i\omega t} \quad (7)$$

$$v_{\alpha \text{tot}} = v_{\alpha} + v_{\alpha 1} e^{ikx - i\omega t} \quad (8)$$

where  $n_{\alpha}$  and  $v_{\alpha}$  are the steady state number density and velocity, respectively, and  $n_{\alpha 1}$  and  $v_{\alpha 1}$  are the perturbed amplitudes. A similar pair of equations can be written for species  $\beta$ .

Substituting these perturbed forms for  $n$  and  $v$ , the continuity equations for the  $\alpha$  and  $\beta$  species become:

$$-i\omega n_{\alpha 1} + i k(n_{\alpha} v_{\alpha 1} + n_{\alpha 1} v_{\alpha}) = 0 \quad (9)$$

$$-i\omega n_{\beta 1} + i k(n_{\beta} v_{\beta 1} + n_{\beta 1} v_{\beta}) = 0 \quad (10)$$

By again using the perturbed number density and velocity equations, the momentum transfer equations are:

$$-i\omega v_{\alpha 1} + i k v_{\alpha} v_{\alpha 1} = \frac{q_{\alpha}}{m_{\alpha}} E \quad (11)$$

$$-i\omega v_{\beta 1} + i k v_{\beta} v_{\beta 1} = \frac{q_{\beta}}{m_{\beta}} E \quad (12)$$

where  $m_{\alpha}$  and  $m_{\beta}$  are the mass per particle for species  $\alpha$  and  $\beta$ , respectively. Note that these equations, and thus the perturbations, are coupled via the electric field. Now, solving the continuity equations for  $n_{\alpha 1}$  and  $n_{\beta 1}$ :

$$n_{\alpha 1} = \frac{k n_{\alpha} v_{\alpha 1}}{(k v_{\alpha} - \omega)} \quad (13)$$

$$n_{\beta 1} = \frac{k n_{\beta} v_{\beta 1}}{(k v_{\beta} - \omega)} \quad (14)$$

and solving the momentum transfer equations, Equations (9) and (10), for  $v_{\alpha 1}$  and  $v_{\beta 1}$ :

$$v_{\alpha 1} = \frac{q_{\alpha} E}{m_{\alpha} i (k v_{\alpha} - \omega)} \quad (15)$$

$$v_{\alpha 1} = \frac{q_{\alpha} E}{m_{\alpha} i(kv_{\alpha} - \omega)} \quad (16)$$

the perturbed amplitudes for both the number densities and velocities can be expressed in terms of the steady-state values of each and the perturbation amplitude of the electric field. By inserting these equations into Gauss's law:

$$ikE = -4\pi(q_{\alpha} n_{\alpha} + q_{\beta} n_{\beta}) \quad (17)$$

one obtains the relation:

$$ikE = -4\pi \left[ \frac{i(kn_{\alpha} Eq_{\alpha}^2)}{(kv_{\alpha} - \omega)^2 m_{\alpha}} + \frac{i(kn_{\beta} Eq_{\beta}^2)}{(kv_{\beta} - \omega)^2 m_{\beta}} \right] \quad (18)$$

Eliminating  $ikE$  from both sides of the equation, and using the definition of the plasma frequency,  $\omega_p^2 = 4\pi \frac{nq^2}{m}$ , the dispersion equation is found to be:

$$1 - \frac{\omega_{p\alpha}^2}{(\omega - kv_{\alpha})^2} - \frac{\omega_{p\beta}^2}{(\omega - kv_{\beta})^2} = 0 \quad (19)$$

where  $\omega_{p\alpha}$  and  $\omega_{p\beta}$  are the plasma frequencies for species  $\alpha$  and  $\beta$ , respectively. This expression is simplified when normalized by  $\omega_{p\alpha}$ :

$$1 - \frac{1}{(\tilde{\omega} - \tilde{v}_{\alpha})^2} - \frac{\gamma^2}{(\tilde{\omega} - \tilde{v}_{\beta})^2} = 0 \quad (20)$$

where  $\tilde{\omega} = \frac{\omega}{\omega_{p\alpha}}$ ,  $\tilde{v}_{\alpha} = \frac{k \cdot v_{\alpha}}{\omega_{p\alpha}}$ ,  $\tilde{v}_{\beta} = \frac{k \cdot v_{\beta}}{\omega_{p\alpha}}$ ,  $\gamma = \frac{\omega_{p\beta}}{\omega_{p\alpha}}$ , and  $\omega_{p\alpha}$  is the plasma

frequency of species  $\alpha$ .

One of the fundamental plasma characteristics predicted by these equations are the cold plasma, or Langmuir, oscillations. Consider the case where species  $\alpha$  is the electron "cloud" of a plasma, and species  $\beta$  is the neutralizing ions, both with no net drift. The mass of the ions is so much greater than that of the electrons, that the ion mass can be approximated as infinite. Since the square of the plasma frequency is inversely dependent on the mass,  $\omega_{p\beta}^2 \approx 0$ . Thus, the dispersion equation reduces to:

$$1 - \frac{1}{\tilde{\omega}^2} = 0 \quad (21)$$

with the solution  $\tilde{\omega} = 1$ , or, in other words,  $\omega = \pm \omega_{p\alpha}$ . This solution has no dependence on  $k$ . So, this oscillation is non-propagating, and therefore independent of wavelength. If  $\omega$ , the temporal frequency of the oscillation, is plotted against  $k$ , the wavenumber, the dispersion curves will be those in Figure 7.

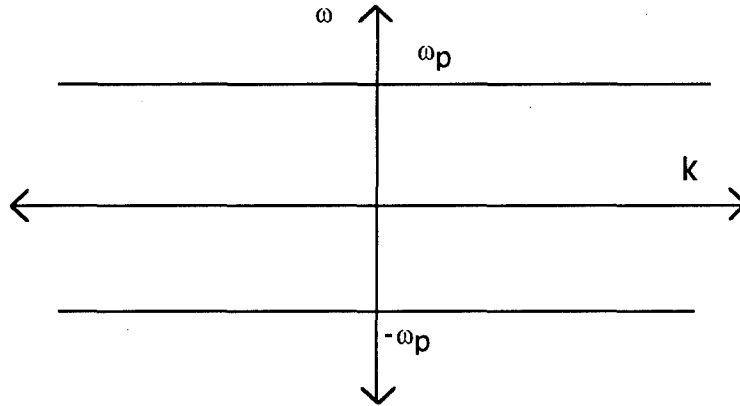


Figure 7: Dispersion Diagram for Cold Plasma Oscillations

If this plasma were drifting at a velocity  $v$ , this picture is altered somewhat. In the frame of the drifting plasma, the electrons are still oscillating at  $\omega_{p\alpha}$ . In the stationary frame, however, there is a Doppler shift of the oscillation. Figure 8 shows the oscillation for drifting plasmas where the plasma is drifting at  $v$  (solid),  $2v$  (dashed), and  $-v$  (dotted). The slope of the lines are the drift velocity of the electrons.

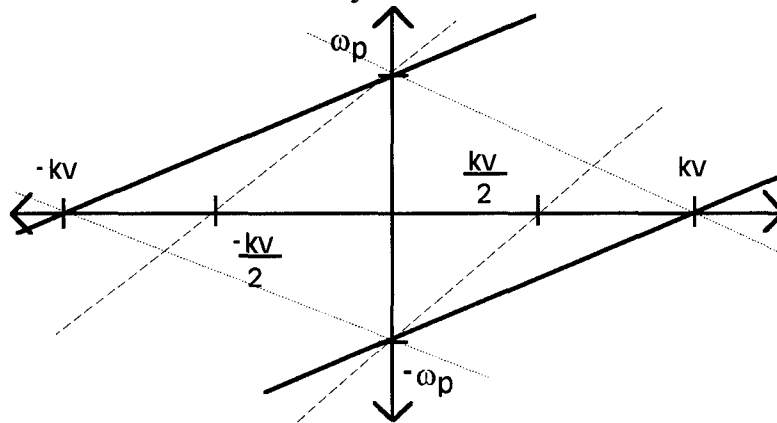


Figure 8: Cold Plasma Oscillations for Drifting Plasmas with Velocities  $v$  (solid),  $2v$  (dashed), and  $-v$  (dotted).

From the independent, single fluid behavior, the next step is to examine the interaction of two fluids. The general form of the dispersion equation, Equation (20)

derived above, is for the two-stream interaction. The most straightforward two-stream interaction is the symmetric case where the two streams are composed of equal densities of electrons and the beams velocities are equal in magnitude, but opposite in direction, the dispersion equation becomes:

$$1 - \frac{1}{(\tilde{\omega} + \tilde{v})^2} - \frac{1}{(\tilde{\omega} - \tilde{v})^2} = 0 \quad (22)$$

where  $\tilde{\omega} = \frac{\omega}{\omega_p}$ , with the solution:

$$\omega = \pm \sqrt{\tilde{v}^2 + 1} \pm \sqrt{4 \cdot \tilde{v}^2 + 1} \quad (23)$$

where  $\tilde{v} = \frac{k \cdot v}{\omega_p}$  and  $v$  is the speed of the electrons.

If the real portion of the solutions are plotted versus  $\tilde{v}$ , the dispersion diagram will be that of Figure 9. The solid lines represent the solutions to the dispersion relation, while the dashed lines are the independent cold plasma oscillations for the drifting beams. As long as  $\tilde{v}$  is sufficiently far from the intersection points of the independent dispersion curves, the behavior of the coupled fluids is close to that of the independent beams. However, as  $\tilde{v}$  approaches the intersection points, the coupling becomes stronger, and the behavior of beams deviate considerably from the independent oscillations.

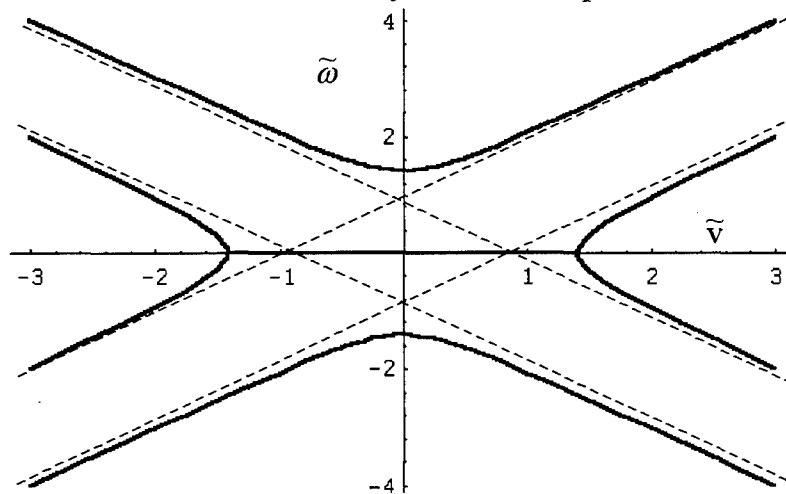


Figure 9: Dispersion Relation for Symmetric Two-Stream Interaction Compared to Drifting Cold Plasma Oscillations.

When  $\tilde{v} < \sqrt{2}$ , two of the solutions become complex. These complex solutions result in an exponential growth in the electric field. The growth rate can be found for different values of  $\tilde{v}$  by plotting the imaginary portion of the solutions versus  $\tilde{v}$ , as in Figure 10. In Figure 10, both complex solutions are included, for both positive and negative  $\tilde{v}$ . Since these solutions are symmetric, all of the necessary information about the instability growth is contained in the first quadrant.

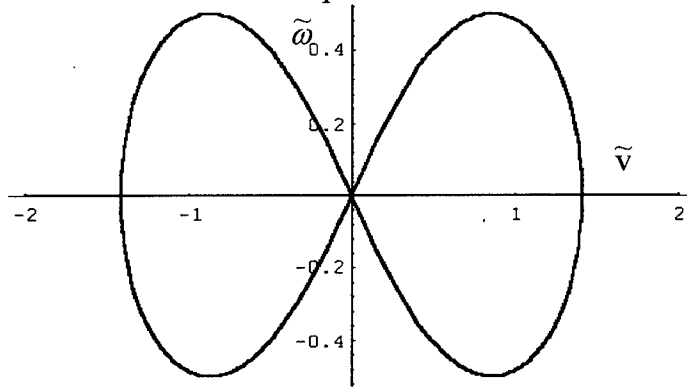


Figure 10: Imaginary Portion of Solutions to the Symmetric Two-Stream Dispersion Relation.

These solutions are a function of the velocity of the beams for fixed values of  $k$ . To examine the behavior of the system with the equations above, it is necessary to determine which values of  $k$  are appropriate. Through a method known as Fourier analysis, a perturbation in the system can be represented as an infinite series of plane-waves of various amplitudes. The set of plane waves used in a Fourier analysis have wavelengths which are an integral number of a fundamental wavelength for the system. These wavelengths are known as the modes of the system. For periodic boundary conditions, there must be an integer number of wavelengths,  $\lambda$ , in the repeat length,  $L$ . Therefore, the allowed modes are such that:

$$\lambda = \frac{L}{N} \quad (24)$$

where  $N$  is an integer, which results in:

$$k_N = 2\pi \frac{N}{L} \quad (25)$$

where  $k_N$  is the wave number of the  $N^{\text{th}}$  mode. So, for the symmetric two-stream case, the  $N^{\text{th}}$  mode will be unstable if:

$$\tilde{v} < \frac{\sqrt{2}}{N} \quad (26)$$

The cutoff point for each mode is therefore inversely proportional to the mode number.

When solving the dispersion relation for various modes, a family of curves such as in Figure 11 can be generated. The curves give the imaginary portion of  $\omega$

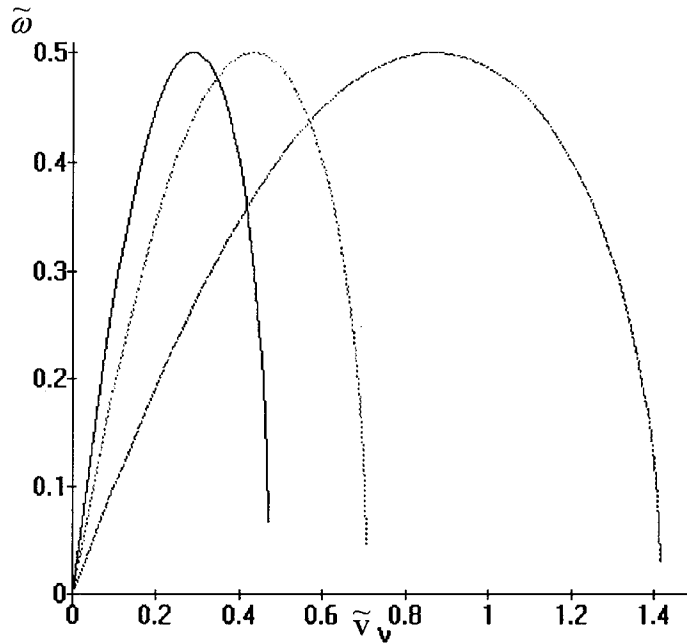


Figure 11: Imaginary portion of  $\tilde{\omega}$  vs. normalized velocity,  $\tilde{v}$ , for modes 1-3, from right to left

scaled by  $\omega_p$  as a function of the normalized velocity. When this value is multiplied by  $\omega_p$ , it gives the growth rate for each mode at the given normalized velocities,  $\tilde{v}$ . For a normalized velocity of 1, for example, a growth in mode 1 of  $0.486\omega_p$  results, but all other modes would be stable. A normalized velocity of  $\frac{\sqrt{3}}{4}$  would result in mode two growing at the fastest rate,  $0.5\omega_p$ , while mode 1 grows at  $0.368\omega_p$  and mode 3 grows at  $0.310\omega_p$ . To recover the velocities appropriate for these numbers, multiply the normalized velocity by  $\frac{\omega_p}{k_1}$ , for the boundary conditions used in this analysis,  $k_1 = \frac{2\pi}{L}$ .

The same kind of examination can be performed with more realistic numbers. Suppose the beams consist of electrons with a total velocity equivalent to the drift of a 1700 K, half-Maxwellian electrons accelerated through a 1V potential, traveling in opposite directions, with number densities of  $5 \times 10^{17} \text{ m}^{-3}$ . For these conditions, a simplification of those present in a thermionic converter, the modes with the highest growth rates are 9 and 10. Because the curves for each mode are so tightly packed in this area, a large number of modes will have nearly equal growth rates, as shown in Figure 12 and Table 1. A small change in conditions will result in a different mode achieving the highest growth rate.

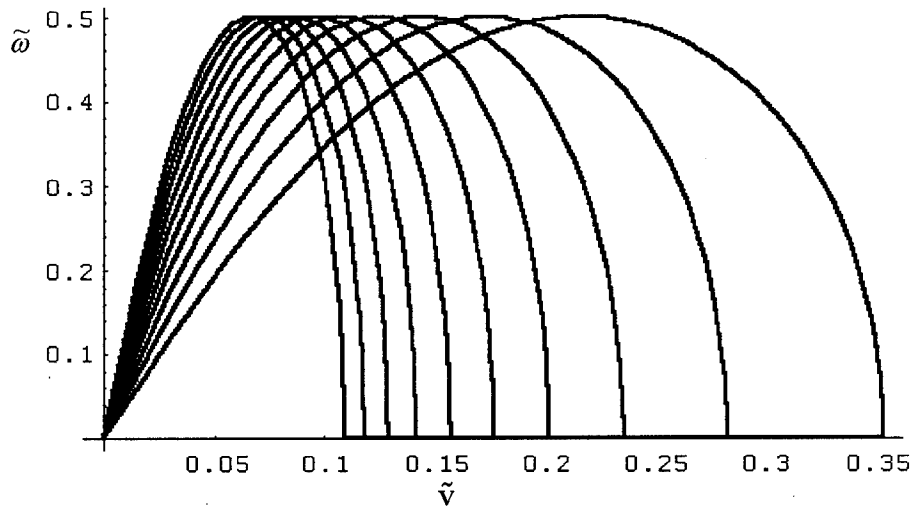


Figure 12: Modes 4-13(right to left) for Two-Stream Instability,  $\gamma=1$

Table 1: Growth Rates for Modes 4-13 for the Two-Stream Instability with  $\gamma=1$

Mode	Growth rate	Mode	Growth Rate
4	$0.329765 \omega_p$	9	$0.499519 \omega_p$
5	$0.387623 \omega_p$	10	$0.496458 \omega_p$
6	$0.433607 \omega_p$	11	$0.479232 \omega_p$
7	$0.467652 \omega_p$	12	$0.445363 \omega_p$
8	$0.489705 \omega_p$	13	$0.389816 \omega_p$

The two-stream interaction can be useful as a tool to understand the changes in behavior when two species are allowed to couple. However, the interaction of most interest for thermionic converters is that of the beam-plasma interaction. This interaction can be thought of a limiting case of two-stream interaction where one stream is no longer drifting. By substituting  $v_{\beta}=0$  into the general dispersion relation of Equation (20), the dispersion relation for the beam-plasma interaction is found to be:

$$1 - \frac{1}{(\tilde{\omega} - \tilde{v}_{\alpha})^2} - \frac{\gamma^2}{\tilde{\omega}^2} = 0 \quad (27)$$

where the quantities are now normalized by the plasma frequency of the beam. When the beam and the plasma are made up of similar particles with the same densities, i.e.  $\gamma=1$ , the solution of the dispersion relation is found to be:

$$\tilde{\omega} = \pm \frac{1}{2} \sqrt{\tilde{v}^2 + 4 \pm 4 \cdot \sqrt{\tilde{v}^2 + 1}} \quad (28)$$

and thus the plasma is stable for all  $\tilde{v} > \sqrt{8}$ . It is interesting to note that both the cutoff value, and the value of  $\tilde{v}$  for maximum growth in the beam-plasma instability are exactly twice that of the symmetric two-stream case examined earlier. Since the relative velocity in the two-stream case is  $2v$ , but it is only  $v$  for the beam-plasma interaction, one can conclude that it is only the relative velocities of the interacting species that is important.

If the solutions to the dispersion relation given by Equation (28) are plotted versus  $\tilde{v}$  and compared to the independent plasma behavior, there are many similarities to the symmetric two-stream case. Figure 13 shows that the coupled solutions (solid) again behave much like the independent cases (dashed) when  $\tilde{v}$  is sufficiently far from the intersection points of the independent dispersion curves, and that the coupling drives the behavior away from the independent behavior as  $\tilde{v}$  nears the intersection points. One major difference from the symmetric two-stream case does show up. The complex solutions are no longer purely imaginary. The solid line crossing diagonally through the origin is the real portion of the complex solutions. The real portion in the complex solution indicates that the wave is now propagating as well as exponentially growing.

However, the growth can still be studied by examining the imaginary portion of  $\tilde{\omega}$  versus  $\tilde{\nu}$  in the first quadrant.

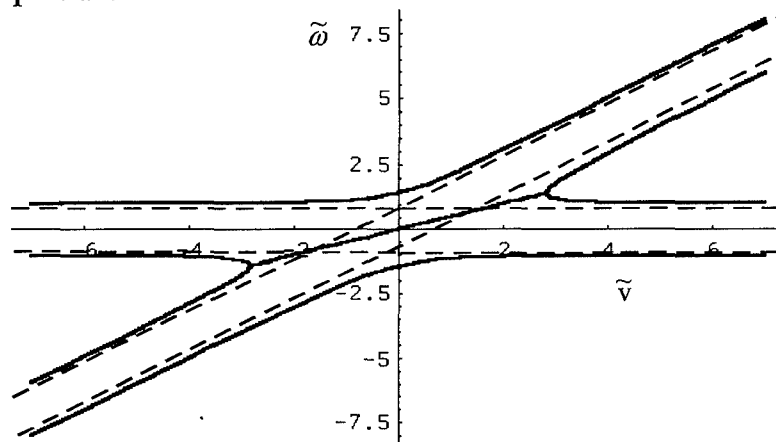


Figure 13: Dispersion Relation Solutions for Beam-Plasma Interaction,  $\gamma=1$ , Compared to Independent Cold Plasma Oscillations.

When the beam and plasma consist of equal densities of electrons, with the beam drifting at  $7.91 \times 10^5$  m/s, equivalent to the average drift of a 1700 K half-Maxwellian beam accelerated through a 1 V potential, the highest growth modes are  $N=18$  and 19. Mode numbers this high mean that the growth curves will be very close together, as shown in Figure 14 and Table 2. These modes are more tightly packed than the fastest

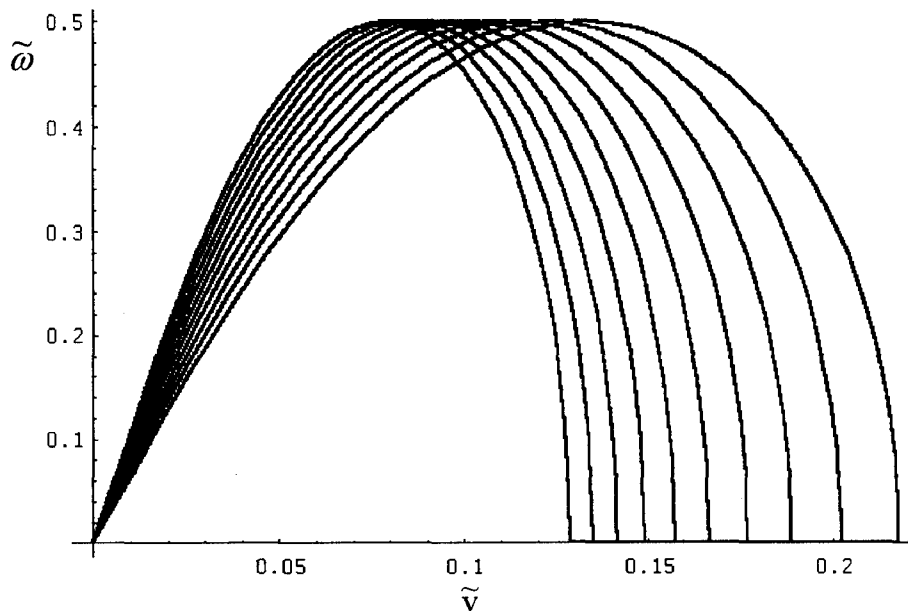


Figure 14: Modes 13-22(right to left) for Beam-Plasma,  $\gamma=1$

modes for the two-stream instability. Therefore, the determination of which mode has the maximum growth rate for the beam-plasma instability will be even more sensitive to changes in conditions than was the case in the two-stream.

Table 2: Growth Rate for Modes 13-22 for Beam-Plasma Interaction with  $\gamma=1$

Mode	Growth Rate	Mode	Growth Rate
13	0.452122 $\omega_p$	18	0.4999519 $\omega_p$
14	0.467652 $\omega_p$	19	0.499658 $\omega_p$
15	0.480186 $\omega_p$	20	0.496458 $\omega_p$
16	0.489705 $\omega_p$	21	0.489733 $\omega_p$
17	0.49617 $\omega_p$	22	0.479232 $\omega_p$

When we consider the beam plasma interaction in a thermionic converter, the number densities of the beam and the plasma are not equal. In a real device, the beam tends to be “weak”, or significantly less dense than the plasma. Therefore, the assumption that  $\gamma=1$  is not a valid one, and the effects resulting from this weakening of the beam must be examined. The when  $\gamma$  is treated as a variable, the solution to the dispersion equation becomes difficult to interpret. It is, therefore, difficult to examine the functional dependence of the dispersion relation on  $\gamma$  directly. Instead, it is possible to calculate solutions for a range of  $\gamma$ . A surface plot, like the plot for mode 1 in Figure 15, of the dependence of the imaginary portion of  $\omega$  on  $\tilde{v}$  and  $\gamma$  can be made for each mode.

With these surface plots, it is possible to see the general trends as  $\gamma$  is increased from the symmetric value of 1, and the beam weakens. As can be seen in Figure 15, as the beam weakens, the range of normalized velocities for which there is growth increases. The maximum growth rate also increases, as does the  $\tilde{v}$  at which this maximum occurs. As shown by Figure 16, for  $\gamma=7.07$  (solid line), typical of the beam-plasma electron densities in a real converter, the peak reaches a value of about 1.2  $\omega_p$  for mode 1 at a normalized velocity of about 7.8. However, remember that the growth rate is

proportional to the plasma frequency of the beam. If the increase in  $\gamma$  is due to a reduction in the beam density, the plasma frequency of the beam is reduced, and therefore the growth rate is reduced.

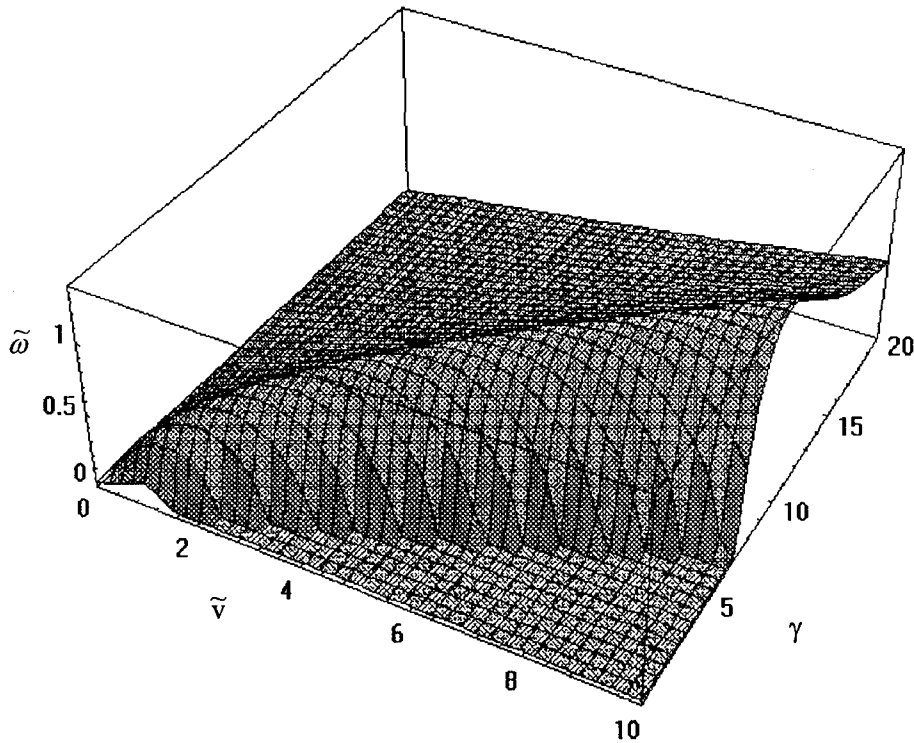


Figure 15: Dispersion surface,  $\frac{\omega}{\omega_{p\alpha}}$ , for beam-plasma interaction.

$\tilde{\nu}$  ranges from 0 to 10, and  $\gamma$  ranges from 0 to 20.

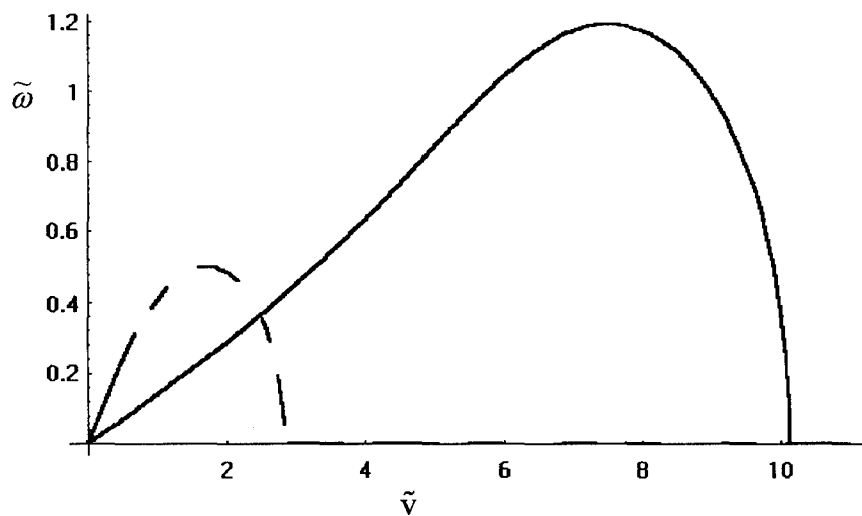


Figure 16: Dispersion curve for beam-plasma interaction for  $\gamma=1$  (dashed), and for  $\gamma=7.07$  (solid).

Now that we have examined the general effects of changing  $\gamma$ , we can calculate the growth rates for conditions more consistent with a real converter. To do this the beam velocity is kept at  $7.9 \times 10^5$  m/sec, but the plasma density is now increased to  $5 \times 10^{19}$  m<sup>-3</sup>, consistent with a thermionic converter in the ignited mode (10:20). This “weak-beam” condition has a noticeable effect on the growth rates. With these new conditions, the highest growth rate now occurs at mode 81. The growth rates for modes 76-85 are given in Table 3 below. In this case,  $\gamma$  is increased to 7.07, and the beam density was not altered from that used in the other calculations in this chapter. Therefore, these growth rates are normalized by the same numbers as those used earlier, and thus the normalized values can be compared directly. So, as is shown in Table 3, the growth rates calculated here are more than twice as fast as those calculated for the equal density case.

Table 3: Growth Rate for Modes 76-85 for Beam-Plasma Interaction with  $\gamma=7.07$

Mode	Growth Rate	Mode	Growth Rate
76	1.17839 $\omega_p$	81	1.19159 $\omega_p$
77	1.18348 $\omega_p$	82	1.19039 $\omega_p$
78	1.18738 $\omega_p$	83	1.18782 $\omega_p$
79	1.19005 $\omega_p$	84	1.18384 $\omega_p$
80	1.19147 $\omega_p$	85	1.17147 $\omega_p$

These calculations allow us to estimate the rate at which the energy of the beam is transferred to the plasma. However, before these rates can be compared to those for collisional relaxation, the theory must be confirmed to be a realistic representation of the behavior of a plasma in a thermionic converter. In Chapter IV, the theory developed here will be verified using several numerical simulations of plasma dynamics.

#### *IV. Comparison with Simulations*

Chapter III established the equations describing the behavior of the two-stream and beam-plasma instabilities. These equations were cast in terms of normalized variables which allow the equations to be applied to a variety of situations with relative ease. The growth rates were calculated first for the symmetric two-stream interaction, and then the beam-plasma interaction. For the beam-plasma interaction, the growth rates were calculated for both the equal density and weak-beam conditions. In this chapter, the analytical results from the previous chapter will be compared to the results of numerical simulations. The basic principles of the numerical simulation will be introduced, and the specific programs used in this project will be briefly discussed. The programs will then be used to verify the predictions made by the fluid theory developed in Chapter III.

It is possible to return to first principles and use Newton's laws and electro-dynamics to perfectly model the plasma and diode. This requires tracking every particle in the system and calculating all the forces acting within it. Since typical plasma densities for these devices are around  $10^{19}$  ions/m<sup>3</sup> with a volume on the order of  $10^{-6}$  m<sup>3</sup>, there are roughly  $10^{13}$  particles to track for just the charged species. At best, this is a difficult and time consuming task. With current computer technology, it is not reasonable to attempt such a solution.

Since it is not possible to directly calculate the motion of each individual particle, it is necessary to make some approximations. The particle-in-cell (PIC) or cloud-in-cell (CIC) technique is commonly used. Instead of tracking all of the particles in the plasma, large super-particles are formed, representing of many particles. These super-particles are then used to approximate the behavior of the collection of particles they represent.

The space of the diode is divided by a grid into discrete, evenly spaced pieces, known as cells. The position of each super-particle is calculated, and the mass and charge

are weighted to this grid based on the particle position. This weighting is used to calculate the electric field, and the force on each super-particle is determined. Then the particle is moved according to the forces calculated. If collisions are to be simulated, Monte Carlo methods are used to determine if there is a collision and what effect it has on the particles involved (2:11-12,255-256).

PIC codes have been proven to be useful ways to study the behavior of plasma diodes (6:495,7:253,121052). Although the representation of particles as super-particles and the division of the diode spacing into discrete cells introduce error, this error can be minimized with the proper restrictions on the cell size and time steps. In order to resolve the electric field, the cell size must be less than the Debye length for the device. The cells may need to be smaller if the phenomenon to be studied takes place on a smaller scale.

To minimize the error from the discrete time steps, two factors must be considered. The first is that only a small fraction of the particles will cross more than one cell each step. Without this condition, a particle could cross an extremum in the electric field without being affected by it. The second factor to be considered is the time scale of the phenomenon to be studied. For instance, in a large device, although the cell transit time may be relatively long, to resolve plasma oscillations, the time step is constrained to values of the order of the plasma period.

A final consideration is the number of particles per cell. It is a good idea to have a large number of particles per cell. This will reduce the noise created when a particle crosses from one cell to the next. However, having a large number of particles per cell can lead to problems if the device is large compared to the cell size, and can slow the calculations considerably.

ES1 and PDP1 are the PIC codes that are used in this study. For a more detailed description of ES1 and the principles of PIC simulations, see the ES1 reference manual and Birdsall's text (2:1-452,14:1-20). A brief description will be given here. The version of ES1 used was XES1 for use in the OpenWindows environment. ES1 is a simulation of

an infinite one-dimensional plasma, using periodic boundary conditions. With periodic boundaries, when a particle exits one side, a particle of the same species is injected with identical velocity from the opposite side.

The initial conditions and particle definitions are provided to the program via input decks. These input decks are ASCII files which the user provides to the program. A sample deck is provided in Appendix A, with a short description of the meaning of each input parameter. For ES1, all of the species-specific parameters are normalized with respect to each other. The specific normalizations are not important, just that they be consistent.

The ES1 environment allows the user to display various diagnostic windows. The diagnostic most important to this study is the electrostatic energy as a function of time. The electrostatic energy diagnostic displays the total as well as the energy density associated with the individual modes found using Fast Fourier Transforms of the electrostatic energy. The number of modes displayed is specified by the user in the input deck (see Appendix A). The code was modified to provide an ASCII output file containing the values for each mode. This output file can then be manipulated to provide the data needed for comparisons.

The other simulation program used was PDP1. PDP1 is a bounded, one-dimensional plasma simulation including an external circuit. The basic PIC methods are identical to those of ES1. Interested readers are referred to the PDP1 reference manual and the copy of the source code (15:1-31).

Like ES1, the user provides the program with the specifics for each run through an ASCII input deck. The input deck for PDP1 is, however, considerably different from the one used for ES1. A sample input deck and a brief description of the parameters is given in Appendix B. The parameters used in PDP1 are not normalized, and are in terms of SI units. This makes simulation of an actual device easier than for ES1, and makes the interpretation of the input deck more straightforward.

PDP1 also provides a variety of diagnostic windows. Unfortunately, none of the diagnostics available allow a numerical comparison to the theory in chapter III. The phase-space plot is the most useful diagnostic of those provided. With the help of Capt. Nichols, a diagnostic was added for the electrostatic energy as a function of position. The noise in this diagnostic for reasonable runs makes this diagnostic only valuable for qualitative analysis of the system.

The next step is to use these simulations to verify the instability predictions arising from the linearized perturbation analysis in Chapter III. Comparisons will be made with both convenient normalized numbers, and then with the parameters characteristic of real thermionic devices. Since ES1 is a periodic simulation, it should support the theory developed in Chapter III very strongly. To test this agreement, ES1 was run for various cases designed to validate the theory. The electrostatic energy mode diagnostics were observed and the data recorded.

In ES1, Fast Fourier Transforms (FFTs) are performed to determine the spectral distribution of energy in the electrostatic field. The growth rates are found by observing the field energy for each mode. Because the field energy is proportional to the square of the electric field, the growth in the field energy is proportional to the square of the growth in the electric field. Therefore, the field energy growth is proportional to  $e^{2\omega_i t}$ , and the growth rate for each mode can be found from the slope of the linear region on the semi-log plot. The code is run and an ASCII dump file is created with the time histories of all of the modes. This file is read into Mathematica<sup>TM</sup> and a linear fit is made. Figure 17 is an example of the fit to one of the modes, in this case mode 1 growth for a symmetric two-stream interaction.

For the symmetric electron-electron two-stream interaction, the location of the transition from a stable to unstable system agreed to within nine decimal places. Runs were made just above and below the cutoff of  $\tilde{v} = \sqrt{2}$ , and the changes observed. When the normalized velocity was above the cutoff, the beams were slightly disturbed, but

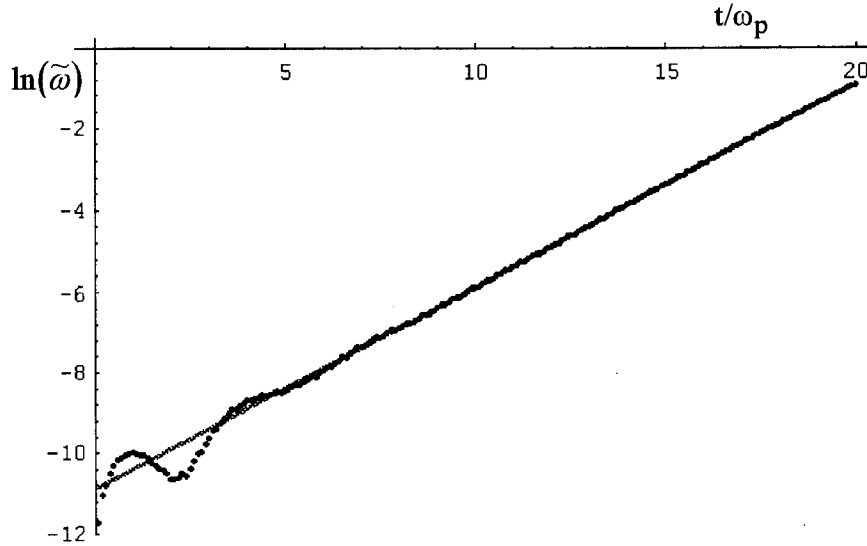


Figure 17: Fit to data for mode 1 growth in ES1  
with  $\tilde{v} = 0.8660$

maintained their overall structure (Figure 18). When the normalized velocity was lowered below the cutoff, nearly complete thermalization of the beams occurred (Figure 19). Both Figure 18 and 19 are snapshots of the screen during a run of ES1.

With confirmation that the theory correctly predicts the stability threshold for the numerical simulation, the growth rates for the instability were tested. Runs were made at strategic points along the curves of the first three modes. The locations were chosen to be: 2 velocities for mode 1 growth alone, the velocity for maximum growth in mode 1, a velocity with mode 1 dominant but mode 2 growing, the velocity for maximum growth in mode 2, and a velocity with mode 3 as the dominant mode. The input deck for ES1 has its variables defined as normalized parameters similar to the  $\tilde{\omega}$  and  $\tilde{v}$  used in the derivations above making a comparison of normalized values easy. However, a problem arose from the method ES1 uses to perturb the system. ES1 stimulates one mode with a small, sinusoidal perturbation, with a magnitude of 0.0001 of the energy of the injected beams for these runs. When this mode was the sole mode growing, the agreement was within a few percent for that mode. The growth rates for the other modes, however, were extremely noisy and very different from those predicted by the theory.

Vx-X Phase Space

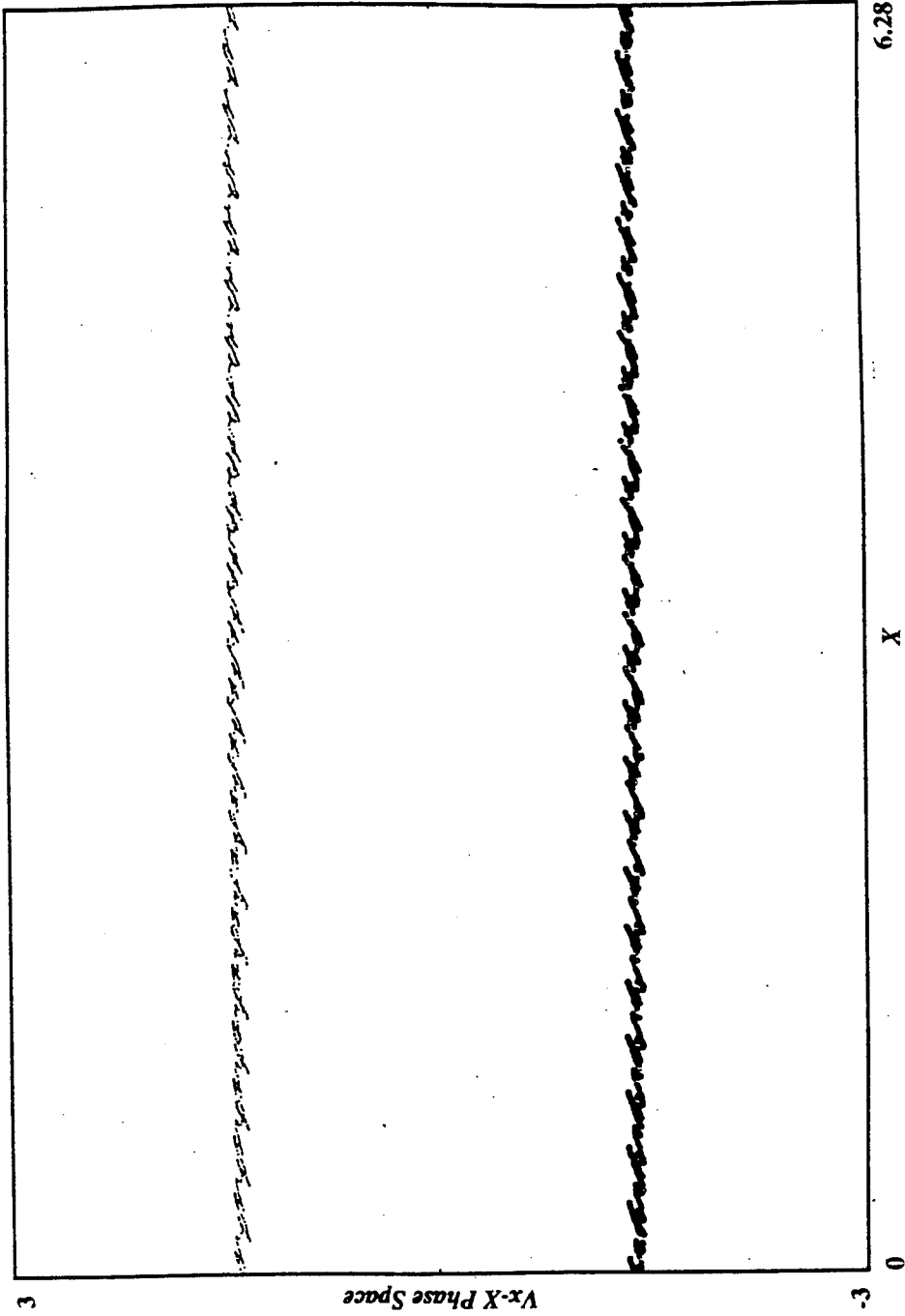


Figure 18: Snapshot of ES1 sub-threshold behavior. Vx-X Phase Space is a plot of particle velocity in the x-direction versus position. The particles have spread slightly from the cold beams, but the beam-like character remains intact.

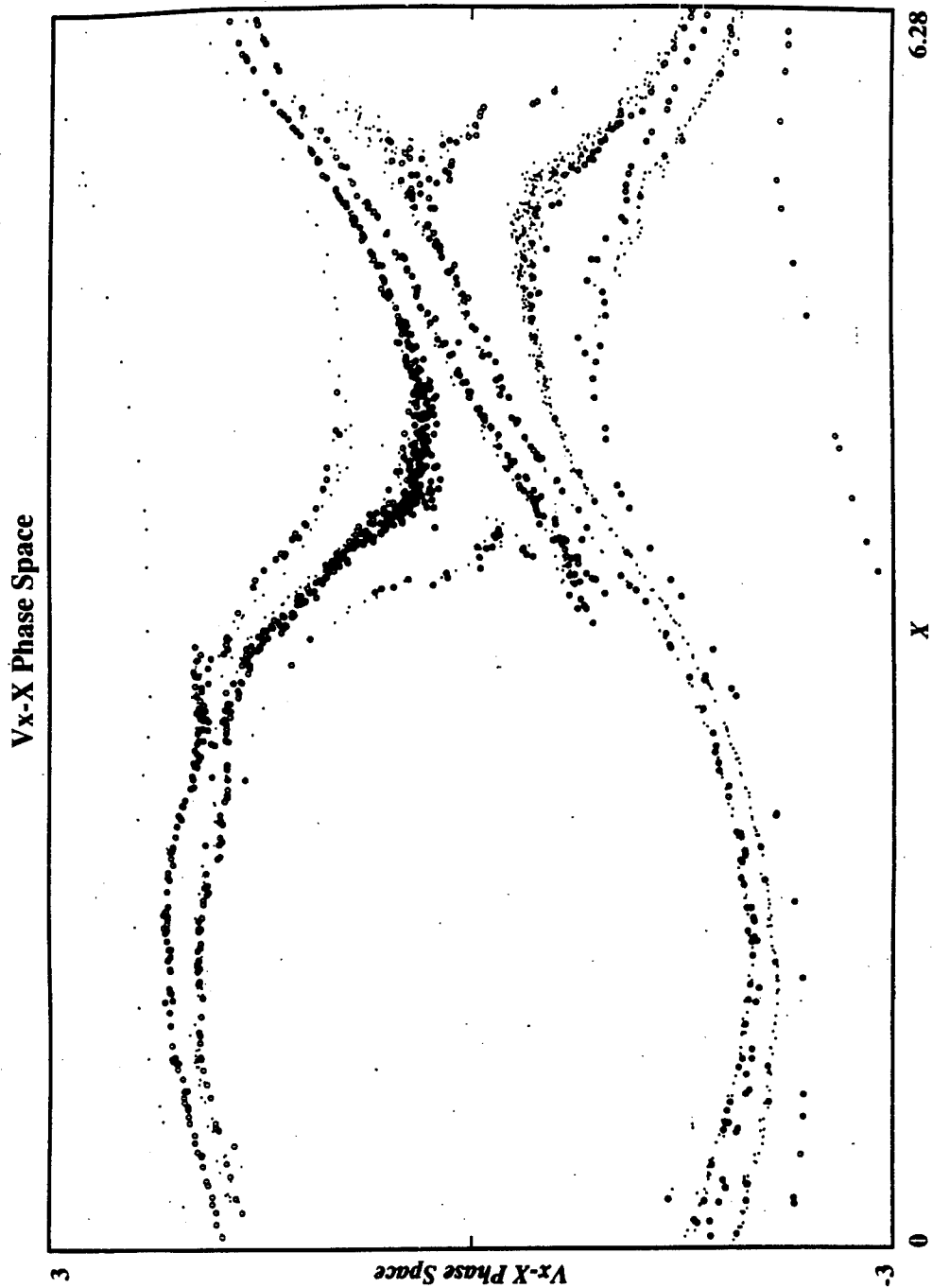


Figure 19: Snapshot of ES1 instability onset. Again, this is a plot in Vx-X phase space. Here, the particles are well spread in velocity and no longer behave as beams.

To address this problem, a routine was created to stimulate all of the modes simultaneously. Because the emission from a heated plate will be uneven, the density and velocity distributions will not be identical at all times. The routine simulates these fluctuations with small, sinusoidal perturbations to the density of the particles. Since the fluctuations are likely to be white noise and thus have a significant amplitudes for a large frequency spectrum, it is not unreasonable to stimulate a large number of modes.

When the code was run with this routine in place, the growth observed in all modes is now consistent with theory. Figure 20 is a contrast of the mode data

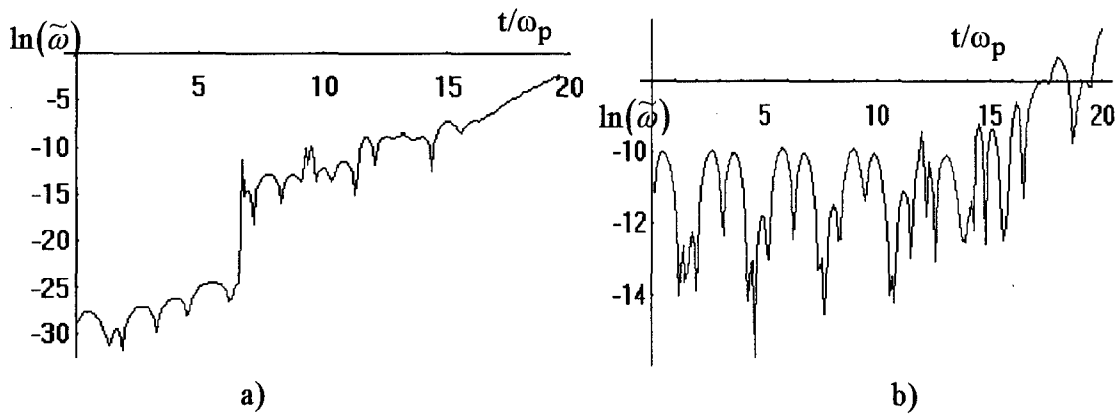


Figure 20: Mode 3 data for two-stream interaction with  $\tilde{v}=1$ ,  $\gamma=1$  and a) only mode 1 stimulated, and b) modes 1-3 stimulated.

with and without the multi-mode stimulation in the logarithm of electrostatic energy density of mode 3 is displayed as a function of time, expressed in terms of plasma periods. Specifically Figure 20a shows the mode 3 data when the normalized velocity was 1 and only mode 1 was stimulated. In Figure 20b, the normalized velocity was again 1, but this time the first three modes were stimulated. Since there is no growth expected in mode 3, the data from the multi-mode stimulation agrees much more strongly with the predictions from the theory. Because the multi-mode stimulation is physically justifiable, the results from runs made with the routine in place can be considered to be an accurate representation of a real system.

The subsequent data runs were all made with the multi-mode stimulation routine in place. Figure 21 compares the growth rate values obtained from the simulation fits to the values predicted by theory. All of these values agreed to within 1% of the theoretical values. The error is easily accounted for in uncertainty in which region to use for the fit.

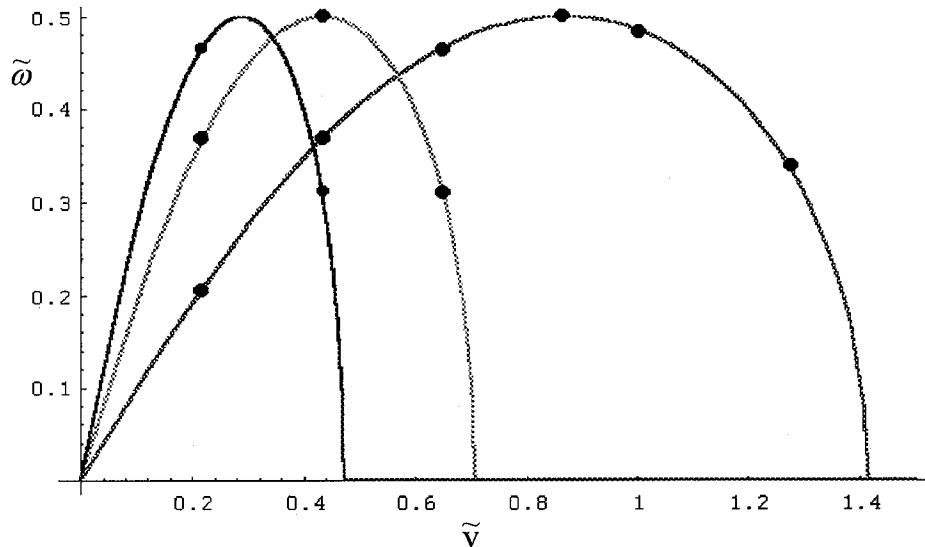


Figure 21: Instability growth rate obtained from fit of simulation data (dots) compared to analytical curves for two-stream interaction,  $\gamma=1$ , modes 1-3.

By changing which portion of the curve was used for the fit, the slope can change dramatically in some cases. The fits giving the data shown above were made using what appeared to be the most linear sections of the data output curves.

The beam-plasma theory was also compared to results obtained from ES1. The growth rates predicted for the beam-plasma instability are given by Equations (27) and (28). A series of runs were performed at evenly spaced normalized velocities with the beam and the plasma both assumed to be electrons and to have the same number density. Table 4 shows the growth rate values obtained for these values and those predicted by theory.

The agreement between simulation and theory for the normalized values allows greater confidence in the growth rates calculated for conditions consistent with thermionic converter operation. Runs were made with numbers consistent with those found in

Table 4: Fit, predicted values and relative error for beam plasma interaction,  $\gamma=1$

$\tilde{\nu}$	Mode	Fit value	Theory	% error
2.2545	1	0.443572 $\omega_p$	0.442306 $\omega_p$	0.2
2.2545	2	*	0	*
2.2545	3	*	0	*
1.414	1	0.482314 $\omega_p$	0.481692 $\omega_p$	0.13
1.414	2	*	0.0141892 $\omega_p$	*
1.414	3	*	0	*
1.00	1	0.405844 $\omega_p$	0.405233 $\omega_p$	0.15
1.00	2	0.484729 $\omega_p$	0.485868 $\omega_p$	0.23
1.00	3	*	0	*
0.8660	1	0.367026 $\omega_p$	0.367127 $\omega_p$	0.03
0.8660	2	0.503222 $\omega_p$	0.5 $\omega_p$	0.64
0.8660	3	0.309831 $\omega_p$	0.3105 $\omega_p$	0.22
0.5774	1	0.265234 $\omega_p$	0.267166 $\omega_p$	0.73
0.5774	2	0.440889 $\omega_p$	0.440692 $\omega_p$	0.05
0.5774	3	0.504536 $\omega_p$	0.5 $\omega_p$	0.91

\* data was too noisy for a reasonable fit.

thermionic converters and compared with those predicted by theory. First, the growth rates will be investigated for a case where the beam and plasma densities are equal. Then the plasma density will be increased to a more realistic value to establish the growth rate for a thermionic converter operating in the saturated regime.

For the equal density case, or  $\gamma=1$ , the runs were made with cold beams with a velocity of  $7.9 \times 10^5$  m/sec, consistent with the drift velocity imparted by a 1V acceleration and a half-Maxwellian velocity distribution with a 1700K temperature. The beam and the plasma had number densities of  $10^{18} \text{ m}^{-3}$ . The individual modes grew as predicted by

theory. The fits matched the growth rates for all the modes checked to less than 1% (Table 5). However, the density of electrons in the beam is not normally equal to that in the plasma. To make any judgment about the accuracy of the theory for a real converter, the weak-beam case must also be tested.

Table 5: Growth Rates for Electron-Electron Beam-Plasma,  
 $\gamma=1$ , modes 13-22

Mode	Fit	Theory	% Error
13	0.450258 $\omega_p$	0.452122 $\omega_p$	0.40
14	0.469353 $\omega_p$	0.467652 $\omega_p$	0.36
15	0.479282 $\omega_p$	0.480186 $\omega_p$	0.19
16	0.486137 $\omega_p$	0.489705 $\omega_p$	0.72
17	0.496789 $\omega_p$	0.49617 $\omega_p$	0.12
18	0.501321 $\omega_p$	0.499519 $\omega_p$	0.36
19	0.497869 $\omega_p$	0.499658 $\omega_p$	0.35
20	0.495932 $\omega_p$	0.496458 $\omega_p$	0.11
21	0.487706 $\omega_p$	0.489733 $\omega_p$	0.41
22	0.475588 $\omega_p$	0.479232 $\omega_p$	0.76

For the weak-beam case, the beam was still considered to have a velocity of  $7.94 \times 10^5$  m/sec and a density of  $10^{18} \text{ m}^{-3}$ , but now the plasma density was set to  $5 \times 10^{19} \text{ m}^{-3}$ , corresponding to a  $\gamma=7.07$ , as might be seen in a thermionic converter in the saturated regime (10:20). Again, the modes grew as predicted, to within 1% of the growth rates calculated from the theory (Table 6).

This confirmation of the unbounded theory for conditions approximating those found in a thermionic converter is not sufficient to answer the original question. In order to determine if the beam-plasma instability plays an important role in a real device, it is necessary to more closely simulate a thermionic converter. This first step in this refinement requires addressing the bounded nature of the plasma in order to evaluate the

Table 6: Growth Rates for Electron-Electron Beam-Plasma,  
 $\gamma=7.07$ , modes 76-85

Mode	Fit	Theory	% Error
76	1.17711 $\omega_p$	1.17839 $\omega_p$	0.11
77	1.18037 $\omega_p$	1.18348 $\omega_p$	0.26
78	1.19341 $\omega_p$	1.18738 $\omega_p$	0.51
79	1.19461 $\omega_p$	1.19005 $\omega_p$	0.38
80	1.19503 $\omega_p$	1.19147 $\omega_p$	0.30
81	1.19521 $\omega_p$	1.19159 $\omega_p$	0.30
82	1.19401 $\omega_p$	1.19039 $\omega_p$	0.30
83	1.18437 $\omega_p$	1.18782 $\omega_p$	0.29
84	1.18126 $\omega_p$	1.18384 $\omega_p$	0.22
85	1.17434 $\omega_p$	1.1784 $\omega_p$	0.34

role of geometric constraints on instability growth. The PDP1 code, unlike ES1, simulates a bounded plasma including the electrical circuit. Unfortunately, PDP1 lacks a diagnostic for the electrostatic energy as a function of position. Without this numerical data, the evaluation and characterization of instability growth can only be made in a qualitative manner.

PDP1 was run for an electron-electron two-stream instability with the same  $7.9 \times 10^5$  m/sec drift velocity used with for the other runs. The finite electrode gap of  $3 \times 10^{-5}$  m was introduced as a geometric constraint. Both electrodes were maintained at the same potential, approximating the weak field condition existing in the bulk plasma. Both beam and plasma distributions were simulated as "cold." Under these conditions, the beam reversed direction in about  $5 \times 10^{-10}$  seconds, and was significantly thermalized in less than  $10^{-9}$  seconds, as demonstrated by the snapshots of the screens in Figures 22 and 23. This confirmed that the instability grew to a significant degree in a short period of time, with instability growth uninhibited by the geometric constraint.

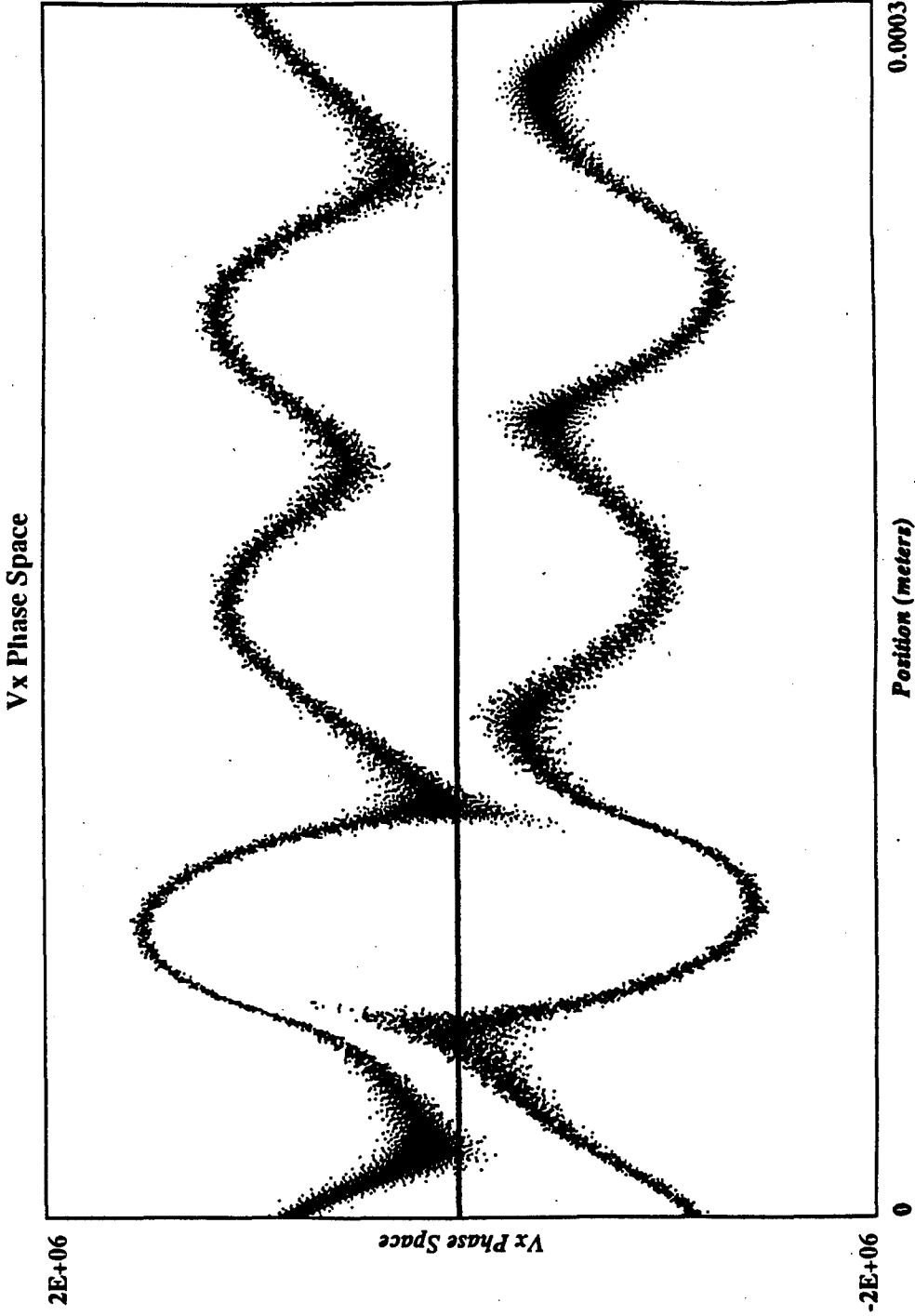


Figure 22: Snapshot of PDP1 run for electron-electron two-stream interaction with  $\gamma=1$ ,  $v=7.9 \times 10^5$  m/sec at  $t=3.98 \times 10^{-10}$  seconds. This is a  $V_x$ - $X$  phase space plot, where velocity in the  $x$ -direction is plotted versus position. The two beams have begun to reverse direction, i.e., cross the zero velocity line, yet they still retain a beam-like quality.

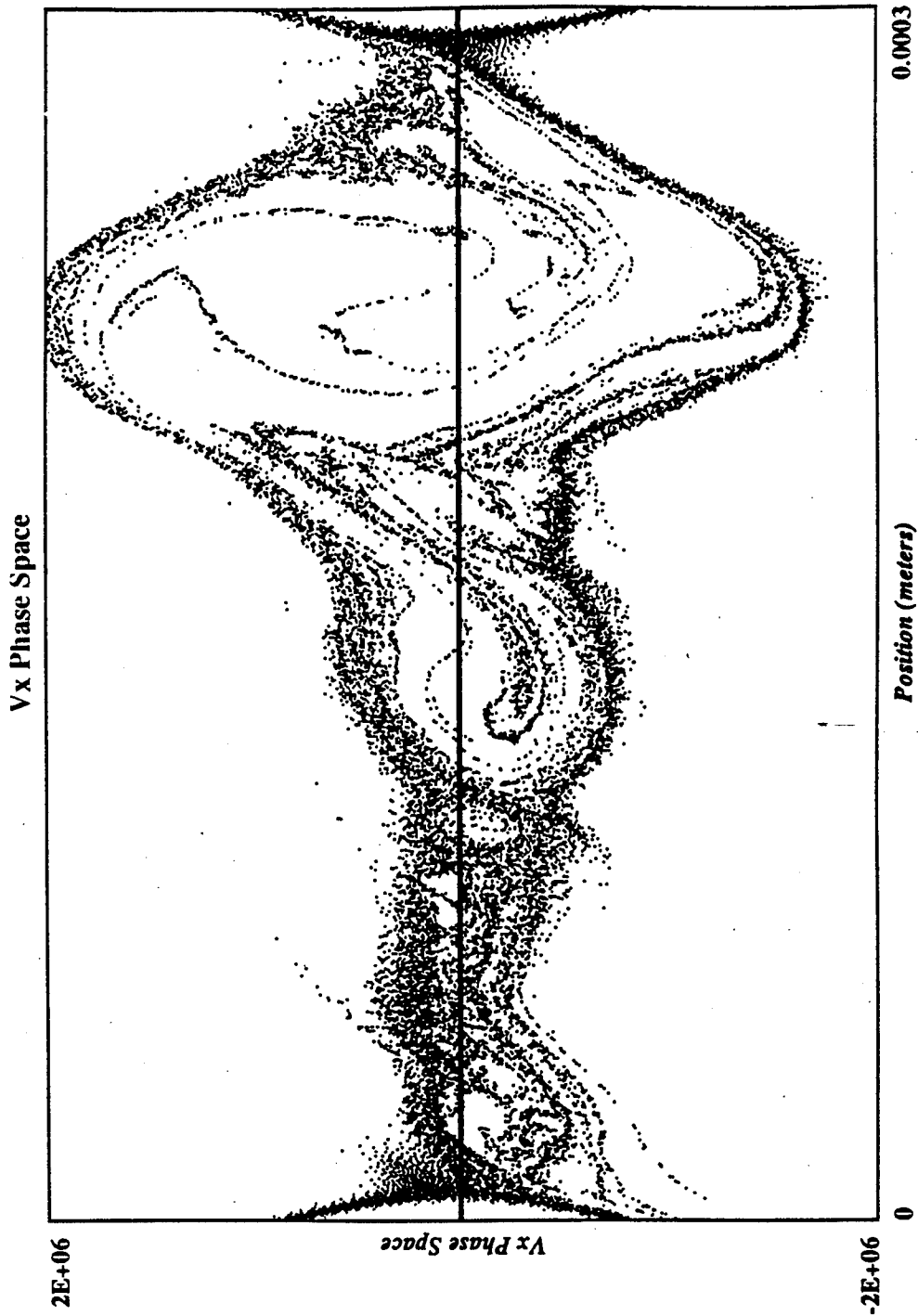


Figure 23: Snapshot of PDP1 run for electron-electron two-stream interaction with  $\gamma=1$ ,  $v=7.9 \times 10^5$  m/sec at  $t=9.96 \times 10^{-10}$  seconds. Again, this is a phase space plot. Here the particles are spread throughout a wide range of velocities, and the beam-like character has been destroyed.

## *V. Discussion and Conclusions*

This study was directed towards an understanding of plasma dynamic processes in a thermionic converter. As was discussed in Chapter II, thermionic converters, currently employed in space power systems, typically operate in the ignited mode, where volumetric ionization is the dominant source of ions in the system. The ions counter the space charge, and form a characteristic potential which can be broken down into three distinct regions. The regions of most interest in this study are the accelerating cathode sheath and the quasi-neutral bulk plasma region. The cathode sheath is typically on the order of 1 V and approximately  $3 \times 10^{-5}$  m wide for a thermionic emission current from a 1700 K cathode of approximately  $10^5$  amps/m<sup>2</sup>. The interelectrode gap is on the order of  $3 \times 10^{-4}$  m. After being accelerated through the 1V potential in the sheath, the injection stream of thermionically emitted electrons has an average velocity of  $7.9 \times 10^5$  m/sec. Through the continuity of current, this results in a beam number density of approximately  $10^{18}$  m<sup>-3</sup> at the cathode sheath-plasma interface. The plasma is typically more dense than the beam, with a plasma density on the order of  $5 \times 10^{19}$  m<sup>-3</sup>, and a temperature of about 0.3 eV. For these typical system values, the collision frequencies for electron-electron collisions and electron-ion collisions are about  $10^9$  and  $10^7$  Hz, respectively (10:20). The electron-neutral collisions are even less frequent and, for the time scales involved in this study, are negligible. The mean-free-path for the electron-electron collisions is on the order of  $7.9 \times 10^{-4}$  m, on the same scale as the interelectrode spacing. Yet when the fluid equations are used by Baksht and others, the collisions are considered to be frequent enough to thermalize the injected stream of electrons in a distance somewhat longer than the cathode sheath (B:84,193-197). It is apparent that this assumption is questionable at best.

If the collisions are not thermalizing the beam, there must be some other interaction causing this thermalization. In this project, collisionless relaxation via the beam-plasma interaction was studied as a possible mechanism. In Chapter III, a linear perturbation analysis was used in conjunction with the fluid equations. The equations were solved for simplified conditions, and the dispersion relation established. With periodic boundary conditions, and the cold plasma approximation, the growth rates were predicted to be on the order of the plasma frequency of the beam for conditions representative of a thermionic converter in the saturated regime. The PIC simulations ES1 and PDP1 were used for verification of these predictions.

The results from ES1 strongly supported the theory for the periodic, cold plasma approximation, with errors on the order of a percent or less. The beam-plasma interaction between the injected stream of electrons and the electrons in the bulk region of the plasma was examined for conditions representative of thermionic converter in the saturated regime. The beam was taken to have a density of  $10^{18} \text{ m}^{-3}$ , resulting in a plasma frequency of  $1.78 \times 10^{11}$ . Since the growth rates were predicted to be on the order of the plasma frequency of the beam, this results in a growth period of about  $7 \times 10^{-11}$  sec. Because the growth period for the instability is at least two orders of magnitude faster than the most rapid collisions, the beam-plasma instability can dominate the thermalization of the injection stream. However, these results are for a simplified view of the system, which neglects geometric constraints and the thermal aspects of both the beam and plasma.

To truly determine whether this instability makes a significant contribution to the thermalization, a more realistic view of the system must be taken. The "obvious" approach would seem to be to run a PIC simulation with all of the real parameters in place. However, a full simulation is not a realistic possibility, and would be of dubious value in examining and parameterizing the physics involved. The size of the time steps in a PIC simulation of a thermionic converter is limited by the plasma frequency and the time

for the fast-moving electrons to cross a cell, leading to time steps of picoseconds or less for a converter in the ignited mode. However, the ions are so much heavier than the electrons that even the most energetic ions are moving at velocities many orders of magnitude slower than the electrons. The run times that would be necessary to allow the ions to reach a steady state within the device would be unreasonably long. In addition to the time constraints, the addition of the full thermal character of the beam and electron plasma can make observing the relaxation behavior of the beam difficult.

The two major aspects that must be examined are the geometric constraints and the thermal nature of the distributions. If the plasma is bounded, the growth may be limited by the transit time of the beam through the interelectrode gap. However, for the conditions in a ignited converter, the transit time is still at least an order of magnitude longer than the growth period for the instability. So, within the limit of the electron transit time, a significant amount of growth can still occur. As a quick test to see if the addition of the boundaries would significantly alter the instability growth, runs were made for with the bounded code PDP1.

The PDP1 runs did confirm that the simplified converter conditions are unstable. These simplified conditions addressed the issue of geometric constraints while retaining the approximation of cold beams of electrons injected from the boundaries at a velocity of  $7.9 \times 10^5$  m/sec, equivalent to the drift of a 1700 K half-Maxwellian accelerated through a one volt potential. Both boundaries were assumed to be at 0 V to approximate the quasi-neutral bulk plasma region. Under these conditions, the beams were significantly thermalized in less than  $10^{-9}$  seconds. Since this is again shorter than the collision times, it is likely that the electron-electron beam-plasma instability plays an important role in thermalizing the injected electrons in the bounded converter plasma.

Setting aside the implications of the bounded nature of the plasma, we now consider the influence of the thermal nature of the distributions on instability growth. The cold plasma approximation does have a significant effect on the growth predicted for the

beam-plasma instability, and must be investigated. With the cold-plasma approximation in place, there is no lower velocity bound for instability growth. In other words, once the velocity is below the stability cutoff for mode 1, the instability will always be growing.

The addition of the thermal distributions will have the most significant impact when the energy in the beam is on the order of the thermal energy in the plasma. As the beam energy is reduced, it becomes more and more difficult to distinguish the beam from the plasma. The efficiency of the energy transfer from the beam to the plasma is thereby reduced, and this will provide a lower velocity bound for the instability growth. In an ignited converter, the plasma temperature is approximately 0.2 to 0.3 eV. As the cathode fall voltage approaches this value, the beam-plasma instability will become less effective at thermalizing the injected stream. The cutoff value for the cathode fall would then be on the order of 0.5V, which places it within the obstructed regime.

With this approximate lower bound, the regions in which the beam-plasma instability can play a role can be defined. The upper bound for the instability growth is approximately that calculated for the cutoff for mode 1. This means that the electrons would have to be traveling with an average velocity on the order of  $2 \times 10^7$  m/sec. Electrons moving at such a velocity would have an energy of 3000 eV, requiring a cathode fall of 3000V. This potential value is well beyond anything that can be developed in a thermionic converter, and therefore the upper bound on velocity is not limiting in thermionic converter relaxation. A lower bound is encountered as the cathode fall is reduced and the beam merges into the thermal distribution of the plasma electrons, the instability growth will be reduced, and finally become insignificant. These conditions will arise in the obstructed regime. Another factor that must be considered in the obstructed regime is the reduction in the number density of electrons in the beam. As the number of electrons capable of crossing the obstruction just in front of the cathode is reduced, the number density in the beam falls off, and, as pointed out in Chapter IV, the growth rate of the instability is reduced.

The beam-plasma interaction therefore plays a role in the thermalization of the injection beam through out the entire saturated regime, and most of the obstructed regime. The effectiveness of the beam-plasma relaxation will diminish and eventually terminate in the obstructed regime. A detailed investigation of the changes in the beam-plasma relaxation due to thermal effects would be a logical follow-up to the current investigation. However, these effects do not appear to be limiting in the saturated regime. Since thermionic converters are typically run at the transition point between the obstructed and saturated regimes, the beam-plasma interaction can dominate the relaxation for most thermionic converters. Therefore, any model of a thermionic converter can not ignore the beam-plasma relaxation mechanism. Because the fluid approaches generally require the assumption of collisionally dominated relaxation, they are inappropriate for describing this relaxation process. In the PIC method, there are no assumptions made about what mechanism is causing the relaxation, and therefore PIC are capable of describing this relaxation. However, using a PIC simulation to model the entire device will result in the run time problems described earlier. To avoid this, a hybrid approach of a PIC simulation of the sheath region mated to a fluid description of the bulk region would be useful. By using the PIC method in the sheath, the collisionless relaxation processes can be modeled. Once the beam has thermalized and entered the bulk region of the device, the approximations made in deriving the collisional fluid equations become justifiable. In the bulk region, the assumption of the Maxwellian velocity distribution is now a good assumption, and therefore the plasma behavior will be well modeled by the fluid approach. The fluid approach greatly simplifies the equations of motion and reduces the computational load. With the hybrid code, the accuracy of the model will be improved over the fluid approach and the computational cost will be greatly reduced compared to a full PIC simulation.

## *Appendix A: Definition of Quantities in the ES1 Input Deck*

A sample ES1 input deck is provided at the end of this appendix.

Definition of quantities in the ES1 input deck (2:31-33):

- nsp:            The number of species to be used in the simulation
- l:                The length of the system. See the explanation for v0.
- dt:              Size of time steps, in units of  $\frac{2\pi}{\omega_p}$ .
- nt:              Maximum number of time steps. Not used in this version of ES1
- mmax:           The maximum number of displayed Fourier modes for the electrostatic energy.
- l/a:             Ratio of length to emitter area. Not used.
- ng:              The number of grid points to be used in the simulation.
- iw:              Weighting to be used, see Birdsall section 2-6: "Particle and Force Weighting" (2:19-22)  
                  2            for first order weighting, used for PIC calculations
- epsi:            Epsilon for the system, in units of  $\epsilon_0$ .
- a1, a2:          Compensation and smoothing factors, respectively. A zero indicates neither is active.
- E0, w0:         External electric field and driving frequency, respectively.

For the individual species, the user must define the following:

- n:                Effectively the number of superparticles to be used for this species.
- nv2:             Exponent for quiet start.
- nlg:             The number of sub-groups to be give the same velocity distribution.
- mode:            When the original code is run, this allows the program to perturb an individual mode. With the added multi-mode stimulation routine, this number is not used.

- wp: The plasma frequency for the species. This quantity can be normalized in any way the user wishes, so long as it is consistent throughout the input deck.
- wc: Cyclotron frequency. Only used for adding a magnetic field.
- qm: Charge to mass ratio. Like the plasma frequency, this can be normalized in any fashion, so long as it is consistent for the input deck.
- vt1: Gives a Gaussian velocity distribution centered on v0. Normalized by the same method as v0.
- vt2: Same as vt1, except is give a "quiet start."
- v0: Drift velocity in the x-direction. This quantity is normalized. It is possible to use the same normalization as was used in this paper:  

$$v0 = \tilde{v} = \frac{2\pi v}{\omega_p L}$$
This is the normalization used for all of the ES1 runs.  
When v0 is defined this way, the value for l given in the input deck is then normalized by k, where  $k = \frac{2\pi}{L}$  with L equal to the real length of the system.
- x1: Magnitude of the perturbation in x. Used as:  $x1 \cos(2\pi \text{Mode}/l +)$ .
- v1: Magnitude of the perturbation in v. Used as:  $v1 \sin(2\pi \text{Mode}/l + \theta_v)$ .
- thetax, thetav:  $\theta_x$  and  $\theta_v$ , respectively.

The charge of the system is found by:  $q = \frac{1}{n \text{ epsi } qm}$

The mass is then calculated by  $\frac{q}{qm}$ , where n, epsi, l, and qm are the quantities defined above.

## BEAM PLASMA INSTABILITY

A cool electron beam is drifting through a cold unperturbed plasma. The small temperature of the beam avoids the non-physical cold beam instability, so the only phenomenon is the growth of the physical beam plasma instability.

```
nsp-----l-----dt-----nt---mmax----l/a
2      6.283185307 0.05    1000  100   0
ng----iw----epsi-----a1-----a2-----E0----w0
1024   2   1.00    0.00  0.00    0     0
```

### SPECIES 1: Cool Electron Beam

```
n----nv2---nlg---mode
2048  0   1   0
wp---wc----qm-----vt1----vt2---v0
1.0  0.00 -1.00 5E-4  0.00 0.0934
x1---v1---thetax--thetav
0.00001 0.00 0.00 0.00
```

### SPECIES 2: Cold Electron Plasma

```
n----nv2---nlg---mode
2048  0   1   0
wp---wc----qm-----vt1----vt2---v0
7.07 0.00 -1.00 0.00  0.00 0.00
x1---v1---thetax--thetav
0.00001 0.00 0.00 0.00
```

## *Appendix B: Definition of Quantities in the PDP1 Input Deck*

A sample PDP input deck is given at the end of this appendix.

The quantities defined here are those necessary to understand the input decks used in this project. For a full description, the reader is directed to the PDP1 reference manual (15:20-27)

nsp:	The number of species in the simulation.
nc:	The number of cells in the simulation.
nc2p:	The number of real particles per superparticle.
dt:	The time step, in seconds.
length:	The length of the interelectrode gap, in meters.
area:	The area of the electrodes, in square meters.
epsilonR:	Permittivity for the system, normalized to $\epsilon_0$ .
B:	Magnetic field strength, in Tesla.
PSI:	Angle (with respect to x) of the magnetic field lines.
rhoback:	Background charge density, in Coloumbs per cubic meter.
backj:	Background current density, in Amps per square meter.
dde:	Sinusoidal perturbation of charge density
extR, extC, extL:	Resistance (in Ohms), capacitance (in Farads), and inductance (in Henries) of the external circuit.
dcramped:	1 means the voltage or current is to be ramped, 0 means no ramping.
source:	A v means a fixed-voltage source, and an i means a fixed-current source.
dc:	Dc voltage(Volts) or current(Amps) for the system
ramp:	Rate at which to ramp up the current or voltage in the system.
ac:	Magnitude of the external alternating current.

**f0:** Driving frequency for the external ac current.  
**theta0:** Phase of driving frequency.  
**secondary:** Turns secondary emission on (1) or off (2).  
**E\_collisional, i\_collisional:** Turns collisions on (1) or off (2) for electrons and ions, respectively  
**reflux:** Turns reflections from the wall on (1) or off (2).  
**nfft:** number of Fast Fourier Transforms to be performed. Caused the program to lock up when used.  
**seec:** Secondary emission coefficient  
**ion species:** Defines the species to be used in ion collisions.  
**Gpressure, Gtemp:** Gas pressure and temperature.

The collision parameters were not used in this project. They are used to define a cross-section with an initial linear ramp to a maximum, a plateau at that maximum, and then an exponential decay (15:24-25).

For the individual species:(all units are SI)

**q:** Charge of species, in Coulombs  
**m:** Mass of species, in kilograms  
**j0L, j0R:** The injection current density from the left and right electrodes, respectively  
**initn:** The initial number density for this species.  
**vx0L, vx0R:** Left and right drift velocities, respectively.  
**vxtL, vxtR:** Thermal velocity to the left and right.  
**vcL, vcR:** Cuts off all lower velocities to the left and right  
**vperpt:** Thermal velocity for the y and z directions  
**nbin, Ebin, Emax:** Used in energy diagnostic at the right wall  
**vperp0:** Drift velocity for y and z.

2 stream(IN SI UNITS)

-nsp---nc---nc2p---dt[s]---length[m]---area[m^2]---epsilon\_r---B[Tesla]---PSI[D]--  
2 500 1e9 1e-12 0.0003 0.004 1.0 0.0 0.0

-rhoback[C/m^3]---backj[Amp/m^2]---dde---extR[Ohm]---extL[H]---extC[F]---q0[C]-  
0.0 0.0 0.0 0.0 0.0 1.0 0.0

-dcramped--source--dc[V|Amp]--ramp[(V|Amp)/s]---ac[V|Amp]---f0[Hz]--theta0[D]-  
0 v 0.0 0.0 0.0 0.0e7 0.0

--secondary----e\_collisional----i\_collisional----reflux---nffi--  
0 0 0 0 0

--seec(electrons)---seec(ions)---ion species----Gpressure[Torr]---GTemp[eV]---  
0.0 0.0 2 3e-2 0.026

ELECTRON-NEUTRAL COLLISIONAL PARAMETERS-----

--selsmax[m^2]---elsengy0[eV]---elsengy1[eV]---elsengy2[eV]-  
1.2e-19 0.0 0.0 20.0

--sxtmax[m^2]---extengy0[eV]---extengy1[eV]---extengy2[eV]---  
7.0e-21 11.55 30.0 100.0

--sionmax[m^2]---ionengy0[eV]---ionengy1[eV]---ionengy2[eV]---  
3.0e-20 15.76 30.0 100.0

ION-NEUTRAL COLLISIONAL PARAMETERS-----

---achrgx[m^2]--bchrgx[m^2/V^1/2]-----ascat[m^2]--bscat[m^2/V^1/2]---  
2.0e-19 0.0e-19 1.8e-19 0.0e-19

SPECIES 1

---q[C]-----m[Kg]---j0L[Amp/m^2]---j0R[Amp/m^2]---initn[m^-3]--  
-1.602e-19 9.11e-31 1.27215e5 1.27215e5 2e18

--vx0L[m/s]---vx0R[m/s]---vxtL[m/s]---vxtR[m/s]--vxcL[m/s]--vxcR[m/s]---  
7.94e5 7.94e5 5e4 5e4 0.0 0.0

---vperpt[m/s]---vperp0[m/s]---nbin----Emin[eV]----Emax[eV]  
0.0 0.0 50 0 200

SPECIES 2

---q[C]-----m[Kg]---j0L[Amp/m^2]---j0R[Amp/m^2]---initn[m^-3]--  
1.602e-19 2.206 0.0 0.0 2e18

--vx0L[m/s]---vx0R[m/s]---vxtL[m/s]---vxtR[m/s]--vxcL[m/s]--vxcR[m/s]---  
0 0.0 0.0 0.0 0.0 0.0

---vperpt[m/s]---vperp0[m/s]---nbin---Emin[eV]---Emax[eV]  
0.0 0.0 50 0 200

## References

1. Baksht, F.G., *et. al.*, *Thermionic Converters and Low-Temperature Plasma*, Technical Information Center, U.S. Department of Energy, 1973.
2. Birdsall, Charles K. and A. Bruce Langdon, *Plasma Physics via Computer Simulation*, McGraw-Hill, St. Louis, 1985.
3. Dawson, J.M., "Thermal relaxation in a one-species, one-dimensional plasma", *Phys. Fluids* Vol 7: 419-425, March 1964.
4. Kaibyshev, V. Z., Executor, *Joint Russian American Enterprise "Intertek:" Study of the Possibility of Using Additional Plasma Research Methods. Evaluation of the Applicability of Equilibrium Thermodynamics for Determining the Relative Concentrations of Cesium Atoms and Ions in Their Fundamental and Excited States*, Survey, Moscow, 1993.
5. Krall, Nicholas and Alvin W. Trivelpiece, *Principles of Plasma Physics*, San Francisco Press, San Francisco, CA, 1986.
6. Kuhn, S. "The Physics of Bounded Plasma Systems (BPS's): Simulation and Interpretation," *Contrib. Plasma Phys.* Vol 34, No. 4: 495-538, 1994.
7. Lawson, William S., "Particle Simulation of Bounded 1-D Plasma Systems," *J. of Comp. Phys.* Vol 80: 253-276, 1989.
8. Nasser, Essam, *Fundamentals of Gaseous Ionization and Plasma Electronics*, Wiley-Interscience, New York, 1971.
9. Nichols, Don F., "Space Nuclear Reactor Integration Study," *Proceedings of the 25th Intersociety Energy Conversion Engineering Conference*, Vol 1: 94-99, 1990.
10. Nichols, Don F., *A three Region Analysis of a Bounded Cesium Plasma Using Particle in Cell and Fluid Techniques*, PhD dissertation, School of Engineering, Air Force Institute of Technology (AU), Wright-Patterson AFB OH, September 1994.
11. Razor, Ned S., "Chapter 5: Thermionic Energy Conversion," *Applied Atomic Collision Physics, Volume 5*, edited by H. Massey, E. McDaniel, and B. Bederson, Academic Press, New York, 1982.

- 12 Schwager, L.A., and C. K. Birdsall, "Collector and Source Sheaths of a Finite Ion Temperature Plasma," *Phys. of Fluids B* Vol 2, No. 5: 1057-1068, May 1990.
- 13 Seshadri, S. R. *Fundamentals of Plasma Physics*, American Elsevier Publishing Company, Inc., New York, 1973.
14. Verboncoeur, John P., and Vahid Vahedi, *ES1 Electrostatic 1 Dimensional Code Reference Manual, DOS version 3.0*, Regents of University of California, Berkeley, CA, 1989.
15. Verboncoeur, John P., et. al. *PDP1 Plasma Device Planar 1 Dimensional bounded Electrostatic Code Reference Manual, DOS version 2.0*, Regents of University of California, Berkeley, CA, 1990.

*Vita*

Lieutenant Bret B. Kreh [REDACTED] 79. In 1988, he was awarded a four-year Air Force Reserve Officer Training Corps scholarship in Mathematics. He attended the Pennsylvania State University, where he had a double major in Mathematics and Physics. While there, he worked for a year at the Applied Research Lab evaluating a simulation code for underwater acoustics as a Math honors student. His scholarship was extended for an extra semester, and in January 1993, he was awarded a B.S. in both Mathematics and Physics. After receiving his commission, he was assigned to the Air Force Institute of Technology. He entered the Applied Physics Master's degree program there in June of 1993.

Permanent Address: [REDACTED]  
[REDACTED]

# REPORT DOCUMENTATION PAGE

Form Approved  
OMB No. 0704-0188

Public reporting burden for this collection of information is estimated to average 1 hour per response, including the time for reviewing instructions, searching existing data sources, gathering and maintaining the data needed, and completing and reviewing the collection of information. Send comments regarding this burden estimate or any other aspect of this collection of information, including suggestions for reducing this burden, to Washington Headquarters Services, Directorate for Information Operations and Reports, 1215 Jefferson Davis Highway, Suite 1204, Arlington, VA 22202-4302, and to the Office of Management and Budget, Paperwork Reduction Project (0704-0188), Washington, DC 20503.

1. AGENCY USE ONLY (Leave blank)	2. REPORT DATE <b>Dec 94</b>	3. REPORT TYPE AND DATES COVERED <b>Master's Thesis</b>
----------------------------------	---------------------------------	--

4. TITLE AND SUBTITLE <b>Analysis of Instability Growth and Collisionless Relaxation in Thermionic Converters Using 1-D PIC Simulations</b>	5. FUNDING NUMBERS
--	--------------------

6. AUTHOR(S) <b>2Lt Bret B. Kreh</b>
---

7. PERFORMING ORGANIZATION NAME(S) AND ADDRESS(ES)  <b>Air Force Institute of Technology 2950 P Street Wright-Patterson AFB, OH 45433-7765</b>	8. PERFORMING ORGANIZATION REPORT NUMBER
--	--

9. SPONSORING/MONITORING AGENCY NAME(S) AND ADDRESS(ES) <b>Dr. Frank Thome NMERI TOPAZ 901 University Blvd SE Albuquerque, NM 87106</b>	10. SPONSORING/MONITORING AGENCY REPORT NUMBER  <b>Dr. Alan Garscadden WL/POOC Wright Patterson AFB, OH 45433</b>
--	---

11. SUPPLEMENTARY NOTES
-------------------------

12a. DISTRIBUTION / AVAILABILITY STATEMENT  <b>Approved for public release; distribution unlimited</b>	12b. DISTRIBUTION CODE
--	------------------------

13. ABSTRACT (Maximum 200 words)  <b>This work investigates the role that the beam-plasma instability may play in a thermionic converter. The traditional assumption of collisionally dominated relaxation is questioned, and the beam-plasma instability is proposed as a possible dominant relaxation mechanism. Theory is developed to describe the beam-plasma instability in the cold-plasma approximation, and the theory is tested with two common Particle-in-Cell (PIC) simulation codes. The theory is first confirmed using an unbounded plasma PIC simulation employing periodic boundary conditions, ES1. The theoretically predicted growth rates are on the order of the plasma frequencies, and ES1 simulations verify these predictions within the order of 1%. For typical conditions encountered in thermionic converters, the resulting growth period is on the order of <math>7 \times 10^{-11}</math> seconds. The bounded plasma simulation PDP was used to evaluate the influence of finite geometry and the electrode boundaries. For this bounded plasma, a two-stream interaction was supported and resulted in nearly complete thermalization in approximately <math>5 \times 10^{-10}</math> seconds. Since the electron-electron collision rate of <math>10^9</math> Hz and the electron atom collision rate of <math>10^7</math> Hz are significantly slower than the rate of development of these instabilities, the instabilities appear to be an important relaxation mechanism.</b>
--

14. SUBJECT TERMS <b>Thermionic converters, plasma diodes, collisionless relaxation plasma instabilities, 1-D PIC simulation</b>	15. NUMBER OF PAGES <b>68</b>
17. SECURITY CLASSIFICATION OF REPORT <b>unclassified</b>	16. PRICE CODE

17. SECURITY CLASSIFICATION OF REPORT <b>unclassified</b>	18. SECURITY CLASSIFICATION OF THIS PAGE <b>unclassified</b>	19. SECURITY CLASSIFICATION OF ABSTRACT <b>unclassified</b>	20. LIMITATION OF ABSTRACT <b>UL</b>
--	---	--	---